NOTICE: this is the author's version of a work that was accepted for publication in Remote Sensing of Environment. Changes resulting from the publishing process, such as peer review, editing, corrections, structural formatting, and other quality control mechanisms may not be reflected in this document. Changes may have been made to this work since it was submitted for publication. A definitive version was subsequently published in Remote Sensing of Environment, Volume 124, September 2012, Pages 427-443, http://dx.doi.org/10.1016/j.rse.2012.05.023

Independent patterns of water mass anomalies over Australia from satellite data and models

E. Forootan[a], J.L. Awange[b,c], J. Kusche[a], B. Heck[c], A. Eicker[a]

[a]*Institute of Geodesy and Geoinformation, Bonn University, Bonn, Germany*
[b]*Western Australian Centre for Geodesy and The Institute for Geoscience Research Curtin University, Australia*
[c]*Geodetic Institute, Karlsruhe Institute of Technology (KIT), Engler-Strasse 7, D-76131, Karlsruhe, Germany*

Abstract

The Gravity Recovery and Climate Experiment (GRACE) products allow the quantification of total water storage (TWS) changes at global to regional scales. However, the quantity measured by GRACE represents mass signals integrated over vertical columns, requiring their separation into their original sources. Such a separation is vital for Australia, for which GRACE estimates are affected by leakage from the surrounding oceans. The independent component analysis (ICA) method that uses higher-order statistics, is implemented here to separate GRACE-derived water storage signals over the Australian continent from its surrounding oceans, covering October 2002 to May 2011. The performance of ICA applied to GRACE is then compared to the ICA of WaterGAP Global Hydrology Model (WGHM) and the ICA of the Australian Water Resources Assessment (AWRA) system. To study the influence of rainfall variability on the derived independent patterns, use is made of Tropical Rainfall Measuring Mission (TRMM) data set, from January 2000

Email address: forootan@geod.uni-bonn.de (E. Forootan)

to May 2011. Implementing ICA on GRACE-TWS showed a remarkable improvement in separating the continental hydrological signals from the surrounding oceanic anomalies which was not achievable using a conventional principle component analysis. Reconstructing the continental TWS changes using only those independent components of GRACE that were located over the continent, showed a high correlation with WGHM-TWS and AWRA-TWS. Mass concentrations over the oceans and particularly S2 semi-diurnal aliased pattern were separated as independent modes. Correlation analysis between the independent components of GRACE and climate teleconnections showed that the mass anomalies over the northern ocean, Gulf of Carpentaria and north-eastern parts of Australia were significantly correlated with the El Niño-Southern Oscillation, while those over south and south-eastern parts of Australia were mainly linked to the Indian Ocean Dipole.

Key words: GRACE-TWS, ICA, Signal Separation, Australia

---

1. Introduction

Water availability in Australia is highly variable from year to year, with various parts of the continent (e.g., the southern and eastern regions) having suffered from severe drought conditions during the last decade (e.g., Ummenhofer et al., 2011). These drought episodes have possibly been worsened by higher temperatures (see, e.g., Nicholls, 2004; Ummenhofer et al., 2009; Leblanc et al., 2009). The long-term and inter-annual climate variabilities of Australia are affected by ocean-atmospheric phenomena such as the El Niño-Southern Oscillation (ENSO) (Risbey et al., 2009) and the Indian Ocean Dipole (IOD) teleconnections (Cai et al., 2011). The IOD, for example, normally affects most of East Africa and parts of the Indonesian and Australian regions (Saji et al., 1999), while the ENSO mainly affects the north and east parts of Australia (Nicholls, 1991) and parts of Africa (Becker et al., 2010).

Such variabilities, therefore, affect water availability over large regions of Australia. Implementing a regional hydrological model, for instance van Dijk et al. (2011) showed that during 2006 to 2009, ENSO had a high influence on Australian terrestrial water variations.

Sustainable conservation and management of the Australian water resource, particularly in areas with arid or semi-arid climates, which include many parts of Australia, requires implementing efficient monitoring tool(s) (see e.g., Ellett et al., 2006 and Awange et al., 2009). One such a technique is the Gravity Recovery And Climate Experiment (GRACE) twin satellite mission that routinely observes time-variable gravity signals within the Earth's system (e.g., Tapley et al., 2004a,b). GRACE has found numerous applications in hydrology and ocean sciences, as documented, e.g., in Ramillien et al. (2004), Schmidt et al. (2008), Awange et al. (2008a,b), Werth et al. (2009a) and Chambers (2006).

The possibility of using GRACE monthly gravity field solutions (Tapley et al., 2004) to monitor Australia-wide total water storage (TWS) signals was assessed by Rodell and Famiglietti (1999) prior to the launch of GRACE. This view was continued by Ellett et al. (2006) who showed that GRACE monthly solutions are suitable for monitoring annual and inter-annual groundwater variations in Australia. Leblanc et al. (2009) combined GRACE solutions with hydrological observations and modeling results, and estimated a loss of groundwater from the Murray-Darling Basin (MDB) of 104 km^3 for the period between 2001 and 2007. Chen et al. (2005) found good agreement between the GRACE-based estimates of terrestrial water storage variability for the Victoria Basin and Northern Australia with the values of Global Land Data Assimilation System (GLDAS) hydrological model (Rodell et al., 2004).

Though such possibility of GRACE application to Australian hydrology had been realized, Awange et al. (2009) pointed out that (i) much of Australia has a relatively small TWS signal, which is very difficult to detect using the current GRACE system and processing strategies, and (ii) the effect of considerable spatial and spectral leakage from the surrounding oceans masks the GRACE-derived TWS over the land. Note that the impact of leakage is not the same for different parts of the region. For instance, Tregoning et al. (2008) found a notable land hydrological signal over the Gulf of Carpentaria, while Brown and Tregoning (2010) reported that the hydrological variability over the MDB does not need to account for contamination emanating from other geophysical sources. This result was confirmed by van Dijk et al. (2011) who showed that the dry inland of Australia exhibits little impact from ocean leakage.

Awange et al. (2009) suggested, therefore, that reprocessing of GRACE data tailored to Australia would be desirable for extracting hydrological signals. In this regard, Awange et al. (2011) evaluated a regional solution computed with the mass concentration (*mascon*) method (Lemoine et al., 2007), using the Principal Component Analysis (PCA; von Storch and Zwiers, 1999) and multilinear regression analysis (MLRA) methods. Their study indicated that the mascon products slightly improved the identification of TWS over the Australian continent. The PCA method that was used to extract the large scale spatial and temporal TWS patterns, however, resulted in a clustered behaviour of its derived orthogonal components (e.g., showing seasonal components and trend overlaid in the temporal components). This problem is known as the 'mixing problem' of PCA, which has been addressed in other studies, e.g., in Jolliffe (1989), Hyvärinen (1999a) and Forootan and Kusche (2011).

Furthermore, the condition of water storage in Australia during the last decade, is linked to various climatic factors, such as large-scale atmospheric pressure changes (Nicholls, 2009), higher air temperatures (Nicholls, 2004), Indian Ocean conditions (Cai et al., 2009) and Pacific Ocean variability (Cai and Cowan, 2008). Using the Complex Empirical Orthogonal Function (CEOF) method, for example, García-García et al. (2011) showed that the spreading of the annual water variations from the north to the southeast of Australia are linked to the ENSO and IOD teleconnections.

The successful performance of higher-order decomposition methods such as *Independent Component Analysis (ICA)* (Hyvärinen, 1999 a,b; Hyvärinen and Oja, 2000) for detecting slow dynamic and inter-annual phenomena (e.g., ENSO) from climatic data sets (e.g., surface temperature, sea-level pressure, and precipitation data) was shown by Ilin et al. (2005). Frappart et al. (2010a, b) and Forootan and Kusche (2011) recently applied ICA to decompose GRACE-derived TWS products. In Forootan and Kusche (2011), for example, it is demonstrated that while PCA clusters the GRACE-derived long-term and periodical TWS in several modes, the ICA algorithm, without making prior assumptions about the signal, improves the results.

The present contribution applies the ICA approach of Forootan and Kusche

(2011) to decompose the Australian GRACE-derived TWS data from the GeoForschungsZentrum (GFZ), Center for Space Research (CSR) and Bonn University for the period of October 2002 to May 2011. For comparison, use is made of the WaterGAP Global Hydrology Model (WGHM) (Döll et al., 2003), Australian Water Resources Assessment (AWRA) system (van Dijk and Renzullo, 2011 and van Dijk et al., 2011) and the Tropical Rainfall Measuring Mission (TRMM) precipitation data set (Kummerow et al., 1998). The main objective is to extract statistically independent water storage patterns from satellite observations and models which, we believe, is necessary for better understanding the large scale variability of the Australian hydrology. Once ICA separates the signals over the continent from the surrounding oceans, those independent components that are located over the land will be used to reconstruct the continental water storage changes. This is an important step for comparison and calibration of hydrological models with GRACE-TWS measurements (see e.g., Werth et al., 2009a), in which the leakage of ocean signals on terrestrial signals has not been accounted for. Moreover, the links between the derived independent patterns and ENSO and IOD were also investigated to identify those areas that are controlled by teleconnections and those that are not.

Therefore, ICA was applied to (i) decompose GRACE-derived TWS signals over Australia, and to (ii) decompose WGHM, AWRA and TRMM data sets. The obtained results in (i) were then compared to those of PCA and the individual independent components of (ii). To understand the impact of the climate teleconnections, the correlation coefficients between GRACE-derived independent components of (i) and the ENSO and IOD indices were derived.

This contribution is organized as follows; in section 2, we briefly explain the ICA method starting with a discussion of PCA. The data used in the study are presented in section 3, followed in section 4 by the ICA results from the GRACE, WGHM, AWRA and TRMM data sets for Australia. Section 5 discusses the link between water variability in Australia and the climate teleconnection (ENSO/IOD phenomena). The study is concluded in section 6.

2. PCA and ICA Methods

PCA is a standard data analysis method based on eigenvalue decomposition of the auto-covariance or auto-correlation matrix of a data set. Given an $(n \times p)$ data matrix $\mathbf{X}$, where n is the number of observations over time, and p the number of locations from which the observations are carried out, PCA decomposes the data matrix as

$$\mathbf{X} \simeq \mathbf{P}_j \mathbf{E}_j^T, \quad (1)$$

where $\mathbf{E}_j$ contains the unit length eigenvectors (i.e., empirical orthogonal functions EOFs) in its columns arranged with respect to the magnitude of eigenvalues, $\mathbf{P}_j$ are their corresponding temporal components (i.e., principle components PCs), and $j < n$ is the number of retained dominant modes. A discussion on the selection of the retained modes is addressed in detail, e.g., in Preisendorfer (1988).

ICA represents a 'blind' source separation method based on the assumption of the independence of sources and the non-Gaussian distribution of the observations. 'Blindness' refers to the recovering of source signals from observed mixtures without knowing how they have mixed (Hyvärine, 1999a). Therefore, ICA can be viewed as an extension of PCA (Comon, 1994; Hannachi et al., 2009). While PCA decomposes a spatio-temporal data set (reduced by the long-term average) into sets of orthogonal modes, ICA decomposes it into statistically independent sources. From a statistical point of view, orthogonality and independence are equivalent for Gaussian signals. However, for non-Gaussian signals, independence implies orthogonality, but the reverse is not true (Hyvärine, 1999a,b).

The non-Gaussianity of time series can be computed using the *kurtosis* of time series (Comon, 1994)

$$k = E(\mathbf{x}^4)/E(\mathbf{x}^2)^2 - 3, \tag{2}$$

where $\mathbf{x}$ stands for each time series (columns of $\mathbf{X}$), E is the expectation function that is usually approximated by the time average. For our time series with a length of more than 90 months, a kurtosis greater than 0.5 indicates a non-Gaussian distribution (Westra et al., 2007).

To derive statistically independent components (ICs) from the uncorrelated modes detected by PCA, we follow the ICA algorithm (Fig. 1) proposed in Forootan and Kusche (2011). Similar to Comon (1994), the ICA algorithm is implemented as a rotation method, which involves the PCA approach as the starting point of an iterative process. ICs are computed while a measure of joint statistical independence of the PCA modes is maximized (Cardoso and Souloumiac, 1993).

To this end, fourth-order cumulants (a tensor of quantity indicated by $\mathbf{Q}_{\mathbf{x}}$ in Fig. 1) provide us with a generalized form of the fourth-order moments (Cardoso and Souloumiac, 1993). For time series with Gaussian distributions, all fourth-order cumulants vanish (cf. Papoulis, 1991). Cardoso (1998) showed that when the time series are independent the fourth-order cumulants tensor $\mathbf{Q_x}$ becomes diagonal.

Generally, there are two alternative ways of applying ICA to spatio-temporal data sets (e.g., GRACE-TWS monthly maps) in which temporally independent time series or spatially independent components are estimated (Forootan and Kusche, 2011). Here, we are interested in the spatially independent components since the goal of our analysis is to separate GRACE-derived TWS signals over the Australian continent from the surrounding oceans.

To derive the spatially independent components, the cumulants matrix $\mathbf{Q_x}$ is built using the EOFs of Eq. (1) as discussed in detail in Forootan and Kusche (2011). $\mathbf{Q_x}$ is then decomposed using PCA to provide the initial values for the rotation matrix $\mathbf{R}_j$ used in

$$f(\hat{\mathbf{R}}_j) = \sum_{i=1}^{n^2} (\mathbf{R}_j^T \mathbf{Q_x}(\mathbf{M})\mathbf{R}_j), \qquad (3)$$

where n^2 is the number of the off-diagonal elements, and $\mathbf{M}$ an (arbitrary) $n \times n$ matrix. $\hat{\mathbf{R}}_j$ is an orthogonal rotation matrix that minimizes the off-diagonal elements of $\mathbf{Q_x}$ in Eq. (3) and makes it as diagonal as possible (Cardoso, 1999). Finally, $\hat{\mathbf{R}}_j$ obtained from Eq. (3) is used in Eq. (1), i.e.,

$$\mathbf{X} \simeq \mathbf{P}_j \hat{\mathbf{R}}_j \hat{\mathbf{R}}_j^T \mathbf{E}_j^T = \hat{\mathbf{P}}_j \hat{\mathbf{E}}_j^T, \qquad (4)$$

to rotate the retained modes and make them as spatially independent as possible (Forootan and Kusche, 2011). Finally, $\hat{\mathbf{E}}_j = \mathbf{E}_j \hat{\mathbf{R}}_j$ contains the derived spatial independent components in its columns, while the columns of $\hat{\mathbf{P}}_j = \mathbf{P}_j \hat{\mathbf{R}}_j$ contain their corresponding temporal evolutions. The schematic illustration of the ICA algorithm is shown in Fig. 1.

FIGURE 1

3. Data

3.1. ENSO and IOD indices

Australian inter-annual climate variability is strongly affected by the dominant tropical phenomena, namely the El Niño-Southern Oscillation (ENSO) and the Indian Ocean Dipole (IOD) (Risbey et al., 2009) teleconnections. El Niño is known as a global-scale phenomenon occurring in the ocean and atmosphere, which is counted as the most prominent source of inter-annual variability in the global weather and climate. The ENSO phenomenon consists of an extension of warm weather from the central and eastern tropical Pacific Ocean to Indonesia leading to a major shift in weather patterns across the Pacific (Trenberth and Hoar, 1996). ENSO has long-period (three to eight years) and inter-annual teleconnection rainfall impact mainly over north and eastern Australia (Cai et al., 2011).

ENSO is usually measured by a simple index which represents a large-scale oscillation of the air mass between the southeastern tropical Pacific and the Australian-Indonesian region (Ropelewski and Jones, 1987). Sustained positive values of the index can be interpreted as indicative of La Niña (drought) conditions, while sustained negative values indicate El Niño (wet) conditions. In this study, we used the monthly Southern Oscillation

Index (SOI) from 2002 to 2011, provided by the Australian Bureau of Meteorology[1], where the pressure differences have been measured between Tahiti and Darwin. It should be mentioned here that there are several ENSO indicators which are computed based on sea surface temperature or pressure data sets. Among of these indices, Nino3.4 is an ENSO indicator with generally stronger correlation to Australian rainfall compared to SOI (e.g., Timbal et al., 2010). In the present contribution, however, SOI was selected in order to enable comparison of our results with those of García-García et al. (2011). The index is scaled using its standard deviation resulting in a unitless time series.

IOD is a coupled ocean and atmosphere phenomenon, a basin-scale mode of sea surface temperature (SST) and wind anomalies, in the equatorial Indian Ocean that affects the climate of Australia and other countries surrounding the Indian Ocean (Saji et al., 1999). An IOD event is an inter-annual variability that usually starts around May or June in Australia, peaks between August and October and then rapidly decays (Australian Bureau of Meteorology). A positive IOD year is associated with the cooler than normal SST in the tropical eastern Indian Ocean near Indonesia, and warmer than normal water in the tropical western Indian Ocean near Africa. A positive IOD results in a decrease of rainfall over parts of Australia. In fact, a negative IOD usually evolves following a positive IOD, with a reverse configuration.

The gradient of the IOD event is termed the Dipole Mode Index (DMI) which is usually considered as a measure of the Indian Ocean influence

[1]http://www.bom.gov.au/climate/enso/

on Atmospheric pressure variabilities (Ajayamohan and Rao, 2008). Our study made use of the available DMI data provided by the Japan Agency for Marine-Earth Science and Technology (JAMSTEC)[1] covering the period from 2002 to September 2010. Similar to the SOI, the DMI pattern is also scaled with its standard deviation to be unitless and multiplied by -1 to be consistent with the previous studies, e.g., García-García et al. (2011).

3.2. GRACE solutions

The GRACE satellites were launched on 17th March 2002 as a joint U.S. National Aeronautics and Space Administration (NASA)/German Aerospace Center (DLR) space mission dedicated to monitoring temporal and spatial variations of the Earth's gravity field on a global scale. GRACE gravity field solutions are generated at regular intervals (e.g., daily to monthly) by several institutions, three of which are used in this study as discussed below.

The GFZ solutions: For this study, we used all available release 4 (RL4) monthly spherical harmonic gravity products from August 2002 to May 2011 computed by the GFZ Potsdam (Flechtner, 2007). These models are derived as fully normalized spherical harmonic coefficients of the geopotential computed to degree and order 120, and have been augmented by the degree-1 term from Rietbroek et al. (2009) in order to account for the variation of the Earth's center of mass with respect to a crust-fixed reference system. Note that the degree-1 values, for the months after Rietbroek et al. (2009)'s study, were extrapolated using its annual and semi-annual dominant frequencies.

The CSR and ITG2010 solutions: Two other data sets from the CSR

[1]http://www.jamstec.go.jp

at the University of Texas, USA (Bettadpur, 2007) and Bonn University, Germany (ITG2010) (Mayer-Gürr et al., 2010) were incorporated in order to validate our findings from GFZ data set. These two solutions are based on the same GRACE L1 (GPS and K-band ranging data) as the GFZ solutions. The CSR solutions are provided as gravitational spherical harmonic coefficients up to degree and order 60, available for the same period as the GFZ products. The ITG2010 solutions have been derived using a different functional model based on short arcs of the satellite orbit, which allows the set-up of full empirical variance-covariance matrices for the observations. Furthermore, daily solutions based on a Kalman filter approach have been calculated as a part of the ITG2010 time series and have been introduced as additional background model for the calculation of the monthly solutions. This different treatment of the background models might cause differences in the solutions provided by the different processing centers. A study by Bonin and Chambers (2011), however, showed no significant discrepancy between the background models in the region around Australia. Therefore we conclude that possible differences between the solutions cannot be contributed to the background modeling. The monthly ITG models are available for the period between September 2002 and August 2009, and are complete to degree and order 120 (Mayer-Gürr et al., 2010)[1].

[1] GFZ and CSR RL04 gravity fields are available from the Information Systems and Data Center (http://isdc.gfz-potsdam.de). ITG2010 gravity fields are available from the website of Astronomische, Physikalische und Mathematische Geodäsie (APMG) group at Bonn University (http://www.igg.uni-bonn.de/apmg/index.php?iditg-grace2010)

3.2.1. Validation of GRACE products over Australia

There have been several studies to validate GRACE signal in the Australian region by independent data sets, from which it can be concluded that GRACE is able to determine geophysically relevant signal over Australia. Tregoning et al. (2009), for example, have found a good correlation of GRACE surface mass variations with vertical crustal deformations as measured by GPS for a permanent GPS site located in Darwin. Kurtenbach (2011) provided correlations of up to 0.6 between the daily ITG2010 solutions and daily height change observations at different Australian GPS sites. Tregoning et al. (2008) have found that the annual amplitude of non-tidal mass changes at the Gulf of Carpentaria estimated from GRACE shows good agreement with tide gauge observations at Groote Eylandt. For the MDB, strong correlations of GRACE inter-annual decrease in total water storage with modelled decreases of groundwater levels were reported by Leblanc et al. (2009). Unfortunately, it has not been possible to validate the GRACE solutions against in-situ measurements of ocean bottom pressure, as no such recorders are available in the oceans around Australia (see Macrander et al., 2010).

3.3. WGHM hydrological model

WGHM (Döll et al., 2003) is the global hydrological part of the WaterGAP (Water-Global Assessment and Prognosis) global model of water availability and use. The WGHM model represents the major hydrological components, such as soil moisture, rainfall, snow accumulation, melting, evaporation, runoff, and the lateral transport of water within river networks. Detailed information about the modeling concept and its corresponding assumptions can be found, e.g., in Güntner et al. (2007). In this study, we used global TWS products provided on a 0.5° by 0.5° grid (with the exceptions of Greenland and Antarctica) covering the period between January 2000 and December 2009. The WGHM model has been previously used, e.g., by Awange et al. (2011) to study the Australian water storage variations. Since WGHM represents, after vertical aggregation and forming temporal anomalies, the same TWS parameter as GRACE-TWS, the two data sets can be directly compared.

3.4. AWRA regional hydrological model

The Australian Water Resources Assessment (AWRA) is a system which combines an operational hydrological model with meteorological and remote sensing data to estimate water storages in the soil, surface water and groundwater (van Dijk and Renzullo, 2011). AWRA water balance, using stream flow data from several catchments and incorporating evapotranspiration measurements along with several remotely sensed parameters, has shown a reliable performance to model Australian hydrological variations (van Dijk et al., 2011). To study the terrestrial water variations using a local hydrological model, therefore, this study applied the same TWS grids covering from January 2000 to December 2010 that have previously been used in van Dijk et al. (2011). Similar to WGHM, TWS changes from AWRA are also directly comparable to GRACE-TWS.

3.5. Tropical Rainfall Measuring Mission

TRMM is a joint NASA/Japan Aerospace Exploration Agency mission, which was designed to monitor and study tropical rainfall in the latitude range ±50° over inaccessible areas such as the oceans and un-sampled terrains (Kummerow et al., 1998, 2000; Huffman et al., 2007). To study the monthly total precipitation over Australia, we used the global average products (3B43), which is derived from TRMM instruments, as well as data from a number of other satellites and ground-based rain-gauge data (Kummerow et al., 2000; Huffman et al., 2007). The 3B43 data[1] is originally provided as mm/hour rainfall, and covers a period from January 1998 to May 2011. We converted the data between January 2002 and May 2011 to mm precipitation for each month. The suitability of using TRMM for studying rainfall patterns over Australia has been assessed e.g., in Fleming et al. (2011) showed good correlation between TRMM and rain gauge data over Australia.

3.6. Data processing

In order to prepare the data sets for analysis, the following processing steps were applied.

- The GRACE spherical coefficients at higher degrees are too strongly affected by correlated noise and are, therefore, smoothed by applying the DDK2 decorrelation filter (Kusche et al., 2009). This filter is anisotropic which makes it difficult to be compared with Gaussian filters; an in-depth discussion about shape of the filter is pointed out in Kusche (2007). Applying DDK2 filter reduces the north-south striping in GRACE monthly solutions (Werth et al., 2009b), which were then

[1]TRMM is available from the Goddard Earth Sciences Data and Information Services Center (http://disc.sci.gsfc.nasa.gov/precipitation)

used to generate the global TWS values according to the approach of Wahr et al. (1998).

- Similar to the GRACE products above, the DDK2 filter was applied to the WGHM, AWRA and TRMM data sets to derive exactly the same spectral content expansion as the GRACE filtered products. Otherwise, the differing smoothness of the data sets would make comparison between the TWS quantities difficult.

- After filtering, all data sets were converted to $0.5° \times 0.5°$ grids.

- From each data set, a rectangular region was selected encompassing Australia, with the latitude between $-44.5°$ to $-10.5°N$ and longitude between $112.5°$ to $154.5°E$.

Each derived monthly map contained 5865 non-zero elements except for the WGHM and AWRA products that had 4083 non-zero elements. Less non-zero elements of WGHM and AWRA is due to the fact that hydrological models do not cover the oceans. The data from GFZ covered 98 months of GRACE solutions, the CSR solutions covered 99 months, while the ITG2010 included 84 months. The solutions of January 2003 and July to October 2004 were excluded from GRACE data during the data processing because of their poor quality (Flechtner et al., 2010). WGHM covers 120 months, AWRA covers 132 months while TRMM covers 124 months.

An overview of the signal root-mean-square (RMS) of the four main data sets (GFZ-TWS, WGHM-TWS, AWRA-TWS and TRMM rainfall) is shown in Fig. 2 in order to compare the signal strength over different regions of Australia. The RMS indicates that the main water storage signal is detected over northern Australia, where GRACE and AWRA showed stronger variability than WHGM and TRMM data sets. According to the RMS in Fig. 2, WGHM showed a weak TWS variability over southern and western Australia except a smaller region of the southwest coast. The TWS variability over southern Australia detected by AWRA was also weaker than GRACE.

FIGURE 2

Before implementing the PCA and ICA methods on the data sets, in order to account for the meridian convergence, an area weighting, with respect to the square root of the cosine of the latitudes, was performed. Then the grid maps were arranged in a matrix with grid points in its rows (same as the matrix $\mathbf{X}$ in Eq. (1)). $\mathbf{X}$ was then centered by reducing the mean from each of the columns and checked for non-Gaussianity using (Eq. (2)).

The derived kurtosis (Eq. (2)) shows that 48.8% of the GFZ, 49% of the CSR, 52% of the ITG2010, 76% of the WGHM, 78% of the AWRA, and 78% of the TRMM grid-point time series exhibit a non-Gaussian distribution. We removed the dominant annual cycle from the data sets and then checked the kurtosis of their residuals. The results indicated that still 38%, 42%, 43%, 51%, 51% and 53% of the inter-annual variabilities of GFZ, CSR, ITG, WGHM, AWRA and TRMM time series respectively exhibit non-Gaussian distribution.

4. Numerical results

4.1. Synthetic example

To show how ICA can help to extract true sources from a superposition (summation) case, we designed a simple simulation before applying the PCA and ICA methods to analyse the real hydrological data over Australia. Let us assume that there are four anomaly concentrations over the north, west, east and southeast of Australia, and that the regions have no overlap with each other. Then we assume that the northern part exhibits only an annual signal while the other parts exhibit a superposition of a low amplitude annual signal and a linear trend (Fig. 3). Synthetic data is then generated by scaling the known spatial anomalies with their corresponding temporal components (see Fig. 3).

Now, both PCA and ICA methods are employed to separate the signals in Fig. 3. The results are presented in Fig. 4, which clearly indicates that the output of the PCA method contains a mixture of both linear trend and annual signals over all regions, while the ICA method succeeds in separating them into the original introduced signals. The mixture behaviour detected in PCA happens because the method maximizes the variance explained by each individual orthogonal component. Therefore, PCA clusters the linear and annual singles in both modes (see Fig. 4, PCA results). The ICA algorithm, however, uses the statistical information contained in the fourth order cumulants to rotate the PCA components (Eq. (4)) so that they are as statistically independent as possible. As a result, the introduced signals (Fig. 3) that have different probability density characteristics are recovered in two different modes (see Fig. 4, ICA results).

FIGURE 3

FIGURE 4

4.2. PCA results from the GFZ data

The PCA method in Eq. (1) was applied on the centered data matrices derived from the GFZ TWS data. The derived eigenvalues along with their corresponding cumulative variance percentages are shown in Fig. 5, GFZ. The graph shows that the first two eigenvalues, corresponding to 57% of the total variance, are dominant and well separated from the rest of the eigenvalues. The other eigenvalues are considerably smaller than the first two, as indicated by the flat shape of the graph (Fig. 5, GFZ).

FIGURE 5

Fig. 6 presents the first 6 PCA components of GFZ-TWS to be compared with the ICA results of Figs. 7 and 8. According to Fig. 5, GFZ, selecting the first 6 components reconstructs about 78.5% of the total variation (see Fig. 5, GFZ). The temporal patterns (PCs) are scaled using their corresponding standard deviations such that they are unitless. The spatial patterns have been multiplied by the standard deviation of their corresponding temporal components and are given in millimeters. Therefore, one can consider each of the spatial patterns as an anomaly map from which each mode of TWS variability is reconstructed by multiplying the spatial patterns with their corresponding temporal components using Eq. (1). This strategy is used for all the decomposition results shown in this paper.

As shown in Fig. 6, the spatial pattern of each PCA component consists of several concentrations of the hydrological signals over land and ocean. This is more evident in the spatial pattern of EOF2 to EOF6. The temporal pattern of PCs (see PCs in Fig. 6) also indicates that the long-term trend along with annual and semi-annual cycles exist in nearly all of the components. Overall, our PCA results contain more mixing behaviour than the one derived in, e.g., Awange et al. (2011) from the GRACE data over Australia. This is probably due to the fact that in Awange et al. (2011), the oceanic signals were masked before the implementation of the PCA method, thus constraining any contamination to the computed PCA modes from the ocean leakage. However, this spatial masking of the mass signals itself could be a source of error that needs to be considered (e.g., Fenoglio-Marc et al., 2007). In this study, we did not mask the GRACE signals over the oceans but instead we implemented ICA, by rotating PCA results (including the continental and oceanic mass signals) towards independence, to spatially separate the mass signals over the continent from the surrounding oceans.

FIGURE 6

4.3. ICA results from GRACE, WGHM, AWRA and TRMM data sets

Implementing the ICA algorithm on the data sets starts by applying PCA (Eq. (1)) as the first step on each data sets before rotating them towards independence (Fig. 1). The eigenvalues of the GFZ, WGHM, AWRA and TRMM data sets along with their corresponding cumulative variance percentages are shown in Fig. 5. Note that implementing ICA on WGHM and AWRA individually verifies the GRACE-ICA results from another perspective. Since

TWS from hydrological models represents the same GRACE-TWS over the lands, theoretically, the result of the decomposition should be comparable to that derived from GRACE. Following this section, we will show that the ICA results from GRACE in several basins are in agreement with the ICA of WGHM and AWRA. Note that the ICA results of TRMM provide additional information on rainfall variability during the study period.

Fig. 5 shows that reconstructing more than 90% of the total variability of the GRACE-TWS required selecting the first 11 PCA components. To reconstruct more than 90% of WGHM, AWRA and TRMM, however, only 5 , 5 and 6 components were needed, respectively (see Figs. 5). The rest 10% of the variance in data sets was assumed to be noise.

The eigenvalue spectrum of the TRMM data set is quite different from those of GRACE, WGHM and AWRA (see Figs. 5, TRMM). For TRMM, only the first component (with 71.3% of total variance) was well separated and the rest of spectrum appears almost flat. For GRACE, WGHM and AWRA the first 2 components with $57\%, 79\%$ and 69% of total variance respectively were dominant.

In order to reduce the sensitivity of the ICA rotation (Eq. (3)) with respect to unequal variance representation of the components, the first 2 dominant modes of GRACE, WGHM and AWRA were rotated first, then respectively their remaining $9, 3$ and 3 components. For TRMM that contained only one dominant component, the ICA method was implemented in a single step using the first 5 components. Constructing the fourth order cumulant matrix $\mathbf{Q_x}$ on the PCA results of each of the four data sets showed that the matrix was not diagonal meaning that the PCA components were not statistically independent (see Fig. 1). The ICA components were, therefore, computed using Eq. (4) for all the data sets.

For brevity from GRACE data sets, we only present the spatial independent patterns of the GFZ-TWS data in Fig. 7. To compare the signal amplitudes, we projected the other GRACE-TWS data sets (from CSR and ITG2010), WGHM-TWS, AWRA-TWS and TRMM rainfall data on to the presented spatial base-functions derived from the ICA of GFZ-TWS (Fig. 7). The derived temporal amplitudes of those products are shown along with the ICs of the GFZ-TWS data in Fig. 8. For TRMM, the results represent only the precipitation amounts over Australia and cannot therefore be directly compared to the TWS values derived from GRACE, WGHM or AWRA. However, projecting the TRMM results along with the TWS values (from GRACE, WGHM and AWRA) provides information about the rainfall contribution in each independent component. For those components that were concentrated over the ocean, the WGHM and AWRA time series were not projected, since hydrological models are limited only to the land and do not cover the oceans. Additional results of ICA application to WGHM, AWRA and TRMM are presented in Figs. 10, 11 and 12, respectively. IC5 of WGHM is not shown here since its corresponding variance magnitude was considerably less than those of the first four components.

FIGURE 7

FIGURE 8

For comparing the ICA results of GRACE over the continent to the hydrological models, first, we selected the independent components $1, 4, 5, 6, 8$

and 10 of Fig. 7 and Fig. 8 (the independent components of GRACE that were located over the Australian continent). Then, GRACE-TWS changes were reconstructed using Eq. (3). The RMS of the results is shown in Fig 9,(A). Comparing Fig. 9, A to Fig. 2, GFZ, it is clear that implementing ICA has considerably isolated the signals of surrounding oceans (e.g., no anomalies over the Gulf of Carpentaria and the eastern oceans can be seen). Fig 9, B shows the differences between the linear trend computed from the ICA-reconstructed GRACE-TWS and AWRA-TWS, covering the period of 2003 to 2011. Comparing to AWRA, GRACE estimated stronger drying trend in northwest Australia, as well as, stronger mass gain in east and northeast Australia. These results confirmed van Dijk et al. (2011)'s findings, but they associated the differences to the unexplained trend in AWRA. The magnitude of the differences derived in Fig. 9, B, however, were less than those of van Dijk et al. (2011), which might be related to the different filtering approaches. Finally, the GRACE-TWS variabilities separated by ICA over the continent were temporally correlated with the time series of WGHM and AWRA from 2003 to 2010 and 2003 to 2011, respectively. The correlation results showed a high agreement between the two hydrological models and the ICA-separated results of GRACE over the continent (see Fig. 9, C and D).

FIGURE 9

FIGURE 10

FIGURE 11

FIGURE 12

Below we present a detailed a detailed comparison between GRACE and the hydrological models (e.g., in term of trend and seasonal components). From Fig. 7, it was seen that the first three components of GRACE show TWS concentrations over the northern part of Australia, where their corresponding ICs show an annual cycle (Fig. 8). Particularly, IC1 isolates the annual signal over north Australia, IC2 represents the oceanic mass over the north of the Gulf of Carpentaria (c.f. Tregoning et al., 2008), and IC3 mainly shows annual mass change over the Timor Sea. The computed long-term linear rates for IC1 and IC2 between October 2002 and January 2011 showed that these regions gained mass at rates of 6 ± 2 $mm/year$ and 5 ± 2 $mm/year$, respectively. Vinogradova et al. (2011) pointed out that the variability detected over the Gulf of Carpentaria may be well related to the self-attraction and loading physics, that is missing e.g., in the Ocean Model for Circulation and Tide (OMCT, Thomas, 2002) which is often removed as a background model during the processing of GRACE products. The computed linear rate for IC3 (Timor Sea) was not statistically significant, showing an almost steady mass balance.

A comparison between the first three ICs of GFZ with the projected temporal evolutions from WGHM, AWRA and TRMM, also showed a good agreement (see Fig. 8). This was, to some extent, evident when the computed RMS in Fig. (2) had a similar concentration with a comparable magnitude over the northern regions. However, IC1 indicates that the signal magnitude of WGHM is still less than that of GRACE. Other studies have similarly shown that WGHM generally tends to have smaller seasonal amplitude than GRACE (see e.g., Schmidt et al., 2008). Comparing to WGHM, projection of

AWRA on IC1 shows that it fits better to IC1 of GRACE. This result confirms van Dijk et al, (2011)'s findings that decomposed GRACE and AWRA signals into their linear trend and seasonal components. Temporal evolutions of TRMM, from projection, shows a 1-month lag between precipitation and mass changes in these areas agreeing with previous studies, e.g., Rieser et al. (2010).

IC1 from WGHM and AWRA, respectively shown in Fig. 10 and Fig. 11, are comparable to IC1 of GRACE in Fig. 7, showing a similar annual TWS signal over the northern regions. IC2 of WGHM represents the southern annual cycle with a 6-month phase difference to the north due to the predominant rainfall season (cf. Rieser et al., 2010). The southeastern part of IC2 from WGHM is comparable to IC6 of GRACE in Fig. 7. IC4 of AWRA shows the same annual signal as WGHM over southern regions. Its signal amplitude, however, is larger than that of WGHM and closer to the GRACE results. The IC1, IC2 and IC3 of TRMM are also related to the rainfall pattern over the northern areas with three separate spatial concentrations (shown in Fig. 12). The derived ICs of TRMM are mostly annual and are comparable with the projected evolutions of TRMM (in Fig. 8) in terms of phase and amplitude (see Fig. 12, middle). These results, individually, confirm our findings in Figs. 7 and 8.

IC4 from GRACE isolates a long-term mass loss along with an annual cycle over the northwestern Australia. A linear regression analysis of the GRACE data from October 2002 to May 2011 shows a rate of loss of -19.2 ± 2 $mm/year$ in the region. The linear rate derived from the projected time evolution of WGHM is around one third of the GRACE linear trend (see IC4 in Fig. 8). The reason can be due to the fact that hydrological models are not designed to represent the trends, rather, their strengths are to illustrate cyclic behaviours. The projected evolution of AWRA on IC4, however, agrees better than WGHM with the GRACE estimate. The linear rate of mass decrease of AWRA over the northwest region was -13.2 ± 2 $mm/year$. The smaller linear rate derived from AWRA has been already reported in van Dijk et al. (2011). IC3 of WGHM (see Fig. 10) shows a mass loss at a rate of -7 ± 1 $mm/year$ over the northwestern regions, which is less than the rate computed from GRACE (see IC4 in Fig. 8). IC3 of WGHM also shows a water loss over the southeastern Australia (i.e., the MDB) at a rate of -8 ± 1 $mm/year$, which was larger than the GRACE estimate (-5.1 ± 1 $mm/year$). IC2 of AWRA confirms IC4 of GRACE by isolating the mass loss over northwest of the continent. IC4 of TRMM (see Fig. 12) localizes the rainfall in the northwestern and western part of the northern Australia showing less precipitation from 2004 to 2006, and a decline in rainfall after the year 2007 in these regions (i.e. the amplitude of annual rainfall in 2004-2006 is considerably less than the other years). TRMM results from 2002 to 2011, however, do not show any significant trend in the integrated amount of precipitation. Considering a long period observation of rain gauges, van Dijk et al. (2011) and McGrath et al. (2012) linked the mass loss in northwest Australia to the dry period ($2003-2010$) after the unusually wet conditions during ($\sim 1997-2001$).

IC5 derived from GRACE in Figs. 7 and 8 represents inter-annual TWS changes along with an increasing rate over the eastern and northeastern parts of Australia due to the 2010-2011 wet conditions. A linear regression analysis of the data from October 2002 to May 2011 shows that the rate of water gain was $12 \pm 2\ mm/year$ (see IC5 in Fig. 8). The computed average TWS change rate from October 2002 to January 2010, the period before the floods, was $7.4 \pm 3.6\ mm/year$. Considering the projected temporal evolutions (IC5 in Fig. 8), amplitude of WGHM is lees than GRACE in this region. This is due to the fact that the dominant annual cycle of WGHM is underestimated as well as the fact that the WGHM data used here does not cover the years 2010 and 2011 when the region exhibits a large mass change. Projected evolution of AWRA on IC5 shows the similar pattern as that of GRACE (see van Dijk et al., 2011)). IC3 and IC5 of AWRA show respectively mass variability over northeastern and eastern Australia, thus confirming GRACE results. The temporal evolution from projection of TRMM indicates the influence of the 2010 rainfall in the region, which was also evident from implementing ICA on TRMM (see IC5 in Fig. 12). The temporal pattern of TRMM is very different from those of GRACE and hydrological models, indicating the importance of using other hydrological parameters in this region. The drought patterns of the eastern regions during 2006 and 2007 can also be identified by IC5 of TRMM.

IC6 of GRACE in Fig. 7 localizes TWS concentrated over the southeast of Australia. The corresponding IC6 (in Fig. 8) shows that the annual cycle is dominant. The temporal pattern of IC6 also contains a considerable inter-annual variabilities in its evolution. The long-term trend of IC6 can be split into three sections; one from 2002 to the last months of 2005 that shows a mass gain of $8.2 \pm 4\ mm/year$, then a decline in mass storage with a rate of $-45.2 \pm 8\ mm/year$ is detected until the starting months of 2007, and finally a mass gain at a rate of 12 ± 4 $mm/year$ to May 2011. From the projected patterns, WGHM and AWRA show the same patterns as GRACE, however, their signal amplitudes are smoother than those of GRACE. The temporal projected pattern of TRMM does not follow the pattern of IC6 of GRACE except for the annual peaks that still show a 1-month lag with GRACE results. IC6 of TRMM, individually, represents the rainfall anomaly over the southeastern regions (see IC6 in Fig. 12).

During the GRACE processing procedure high frequency mass variations, e.g. caused by oceanic tides, are reduced as they cannot be resolved by monthly gravity field solutions. However, current ocean tide models are not accurate enough to fully reduce the tidal signal in the GRACE data (Knudsen, 2003). Due to the sampling characteristics defined by the GRACE orbit configuration, these unmodelled high frequency tidal signals occur in the monthly gravity field solutions at alias periods. One well-recognized example is the S2 semi-diurnal tide, which is mapped onto a 161-day period, and thus does not cancel out in the monthly solutions (Chen et al., 2008, Ray and Luthke, 2006). IC7 of GRACE separates the S2 aliasing effect over the ocean located in the northwest of Australia (Figs. 7 and 8). This pattern was previously reported by Melachroinos et al. (2009) who fitted a predetermined cyclic signal (with a period of 161 days) to the GRACE time series. One of the contributions of this study, therefore, is exploring such a pattern as an independent component without using any predefined deterministic model. Exploring such pattern as an individual mode was not possible using PCA. Fitting a sinusoidal function to IC7 showed a period of 161.4 days, agreeing with the theoretical derivation of Ray and Ponte (2003), and matching the observations of Melachroinos et al (2009).

The water loss in west Australia is summarized in the IC8 of GRACE (see Fig. 7). This pattern is also extended towards the ocean. This shows that the performance of ICA, for separating the relatively lower amplitude signals, is decreased. A linear regression of IC8 shows a rate of $-8.2 \pm 3\ mm/year$ from March 2002 to December 2009. The computed linear rate of GRACE-TWS change in the area during the years 2010 to 2011 was $6 \pm 4\ mm/year$, which was due to the increased precipitation in this period. IC8 also shows an opposite TWS gain over central Australia corresponding to $7 \pm 2\ mm/year$ from March 2002 to December 2009. The projected temporal evolution from WGHM shows similarities in phase with GRACE-IC8, but its amplitude is around one fifth that of GRACE. The same statement is also true for the projected evolution of AWRA with an amplitude of 70% of GRACE-IC8. The temporal evolution of TRMM shows similarity only for the years 2004 to 2006. Our results confirm Rieser et al. (2010)'s study that showed the poor link between the TRMM pattern and the GRACE-TWS changes in the central, western, and eastern parts of Australia.

IC9 and IC10 of GRACE in Fig. 7 show mainly inter-annual mass fluctuations over the ocean in the northeastern and southwestern parts of Australia (with a frequency of 99.7 and 121 days, respectively). Note that the reported frequencies are derived by fitting a sinusoidal cycle. For deriving more reliable results together with their associated uncertainty, one might use advanced methods (e.g., in Schmidt et al., 2008). Finally IC11 localizes the TWS anomaly over southeast Australia. The linear rates of TWS change in these regions were not statistically significant. The temporal evolution of

WGHM derived from its projection on to the spatial pattern of IC8 shows the same temporal pattern in southeast but its amplitude was 60% of that of GRACE. Unlike the GRACE results, no clear TWS anomalies were detected over the southern and western Australia from the ICA of WGHM (see Fig. 10) and AWRA. This can be related to the fact that WGHM and AWRA, according to the derived RMS in Fig. 2, show less TWS variability over these regions. Further research will need to address these differences.

5. Effects of ENSO and IOD on Australia

In the preceding section, the relation between the patterns of GRACE-TWS in different regions of Australia and the values of WGHM, AWRA and TRMM were studied (see Fig. 8). Since the derived GRACE-ICs are spatially independent, one can investigate the water variability of each components individually (without considering the others). This gives the unique opportunity to study the links between climate teleconnections (i.e. ENSO and IOD) and the derived GRACE-ICs.

To this end, first, the ICs of GRACE-TWS from GFZ, SOI, and DMI were smoothed with a 12-month moving average filter and interpolated to a regular monthly time steps covering October 2002 to May 2011 (see Fig. 13). Then, the long-period temporal correlations at 95% level of confidence between ICs and the indices, for the periods of October 2002 to 2011 as well as 2006 to 2011, were computed. Selecting the period 2006 to 2011, besides the study period, for computing the correlations was due to the high influence of teleconnections on the Australian TWS changes (see, e.g., van Dijk et al., 2011). The significant correlation values are reported in Fig. 13. Note that selecting SOI and DMI indices for studying teleconnections as well as the 12-month filter for smoothing were done to make the results comparable with previous studies e.g., García-García et al. (2011).

The correlation results indicate a strong stable influence of ENSO for the period 2006 to 2011 on IC1, IC2, and IC3 (with correlations of 0.57, 0.76, and 0.64, respectively). Computing the long-period correlation coefficients (October 2002 to May 2011) between the first three ICs and SOI index also showed significant correlations of 0.51, 0.71, and 0.61, respectively. These correlations confirm the effect of the tropical ocean-atmosphere variability associated with ENSO rainfall in the northern regions, where IC2 and IC3 (indicating the mass variabilities over the ocean north of Australia) have stronger correlation than the northern land signal (IC1). García-García et al. (2011) and Ummenhofer et al. (2009) reported similar results for the northern region using Complex EOF.

Computed correlations between -DMI and the first three ICs were high in some years, e.g., 2006 and 2009. Their long-period correlation values for October 2002 to May 2011, however, were 0.35, 0.26, and 0.32, respectively. The correlations decreased for the period of October 2002 to May 2011. This might show that the effect of IOD on TWS variations over the northern regions is relatively less compared to that of ENSO.

Correlations of IC4 and IC8 with SOI, show the contribution of ENSO to the short-period mass gain between 2010 and 2011. Their long-period correlation for October 2002 to May 2011, however, were not statistically significant. This statement was also true for the long-period correlation of IC4 and IC8 with -DMI.

The effect of ENSO is also evident in IC5 (i.e., TWS variations in the eastern and northeastern regions) and IC9 (which concentrates over the ocean in east Australia) with a significant correlation of 0.79 and 0.81 with SOI for October 2002 to May 2011. For the same period, the correlation between IC5 and -DMI was -0.36, while the correlation value between IC9 and -DMI was -0.31. These values indicate the less long-period effect of IOD on TWS variations over the eastern and northeastern regions compared to that of ENSO.

A significant influence of IOD from middle of 2005 to 2009 over the south-eastern and southern parts of Australia is shown in IC6 and IC11. The computed correlation between IC6 and -DMI for the period of 2006 to 2011 was 0.82. This correlation, for the same period, between SOI and IC6 was 0.51. The correlation value between IC11 and -DMI for October 2002 to May 2011 was 0.54. This value for IC11 and SOI was 0.44.

Correlation between IC10 and IOD, for the period 2006 to 2011 was 0.53, while in this period no significant correlation with ENSO was found. Note that -DMI is selected for computing the correlations since negative IOD indicates increase in water budget and positive IOD indicates decrease in water budget. Since the spatial anomalies are positive (as they are in Fig. 7, the 6th and 11th patterns), -DMI should follow the pattern of the derived ICs (see Fig. 13). These results confirm the study of Ummenhofer et al. (2009) which shows the effect of the Indian Ocean Dipole in the southern regions (see McGrath et al., 2012).

FIGURE 13

6. Conclusion

In this contribution, large scale statistically independent hydrological patterns over Australia have been extracted from remote sensing data and models using the ICA method. Our results indicate that:

ICA has the capability to isolate the effects of spatial and spectral leakages from the surrounding oceans that mask potential terrestrial hydrological signals detectable by GRACE in a regional case such as Australia with weaker hydrological signal, what was unachievable using mascon or PCA and its ordinary extensions (see e.g., Awange et al., 2011 and PCA results in Fig. 6).

In this study, instead of spatial masking of GRACE-TWS over the oceans before implementing the analysis, we extracted a rectangular region including Australia from GRACE-TWS products, covering October 2002 to May 2011. Then an ICA algorithm (Fig. 1) was implemented on the GRACE time series to spatially separate the continental TWS changes from the surrounding oceans. The results appear to be well separated, while the derived spatially independent patterns are localized over the continent or the oceans (see Figs. 8 and 7). Reconstructing the GRACE-TWS over the Australian continent using the ICs that were located over the land showed a significant high correlation with the TWS time series derived from WGHM and AWRA (see Fig. 9).

Some hidden physical processes such as S2 tidal-aliasing along with other model deficiencies were also detected and localized from the data without fitting any pre-defined deterministic model, which was what was done in previous studies.

Verifying the ICs of GRACE-TWS by implementing ICA on the WGHM and AWRA data sets individually showed good agreement in the results, mainly for the dominant variabilities, e.g., mass change over the top north of the continent or the mass loss over the northwest. We could not, however, find the same patterns of e.g., IC2 of WGHM or IC5 of AWRA summarized in one particular IC of GRACE (IC2 of WGHM or IC5 of AWRA were seen in IC6 and IC8 of GRACE). This was due to the difference between the components of GRACE and the hydrological models (i.e., GRACE components cover both the continental and oceanic signals while those of WGHM and AWRA only cover the continent). For instance, for reconstructing 90% of the GRACE signal, we had to select 11 components while for WGHM and AWRA, selecting only 5 components was enough. Following Eq. (4), implementing the ICA rotation on GRACE was done using the first 2 then the remaining 9 components, while for WGHM and AWRA, this was done by selecting the first 2 then the remaining 3 components (see Section 4.3). Selecting more componets for the GRACE case, therefore, forced the optimization procedure (Eq. (3)) to decompose some less dominant patterns (e.g., over the southeast and southwest) into two modes (e.g., IC6 and IC8). However, the reconstruction of GRACE signal over the continent (Fig. 9, A) showed that the separation from the surrounding oceans was succesful. Comparing RMS of the reconstruction and those of AWRA also showed a good agreement. The derived high temporal correlations with the signals of WGHM and AWRA also confirmed that, although some components are not directly compareable, the reconstruction has performed well (see Fig. 9, A and B).

Studying the correlation between the ICA-localized TWS results with the ENSO and IOD phenomena revealed the influences of the climatic teleconnections on each individual statistically independent hydrological region. As a result, a strong link between SOI and the TWS variations in the northern regions and the relation of the IOD to the eastern and southeastern Australia was established. ICA thus presents an alternative method of analysing the relationship between hydrological changes and climate variabilities.

The presented ICA algorithm might be suitable for analysing other hydrological areas suffering from the leakage of surrounding oceanic signals, and weaker hydrological signals.

Acknowledgement

The authors thank two anonymous reviewers and two corresponding editors P. Minnett and M. Bauer for their helpful remarks which improved considerably the manuscript. We also thank P. Döll for her comments on the hydrological aspects as well as A. van Dijk for kindly providing the AWRA-TWS data set. J.L. Awange acknowledges the financial support of Alexander von Humboldt (Ludwig Leichhardt's Memorial Fellowship), Curtin Research Fellowship and the Australian Research Council (ARC) Discovery Projects funding scheme (project DP087738). He is grateful for the warm welcome and the conducive working atmosphere provided by his host Prof. Bernhard Heck at the Geodetic Institute, Karlsruhe Institute of Technology (KIT). This is a TIGeR Publication No.415.

References

Ajayamohan, R. S., & Rao, S. A. (2008). Indian Ocean Dipole modulates the number of extreme rainfall events over India in a warming environment. J. Meteor. Soc. Japan, 86, 225–229. doi:10.2151/jmsj.86.245.

Awange, J., Fleming, K. M., Kuhn, M., Featherstone, W. E., Heck, B. & Anjasmara, I. (2011). On the suitability of the $4\circ \times 4\circ$ GRACE mascon solutions for remote sensing Australian hydrology. Remote Sensing of Environment, 115 (3), 864–875. doi:10.1016/j.rse.2010.11.014.

Awange, J., Sharifi, M., Baur, O., Keller, W., Featherstone, W., & Kuhn, M. (2009). GRACE hydrological monitoring of Australia: current limitations and future prospects. Journal of Spatial Science, 54 (1), 23-36. doi:10.1080/14498596.2009.9635164.

Awange, J., Sharifi, M., Keller, W., & Kuhn, M. (2008a). GRACE application to the receding Lake Victoria water level and Australian drought. In: Sideris, M. (Ed.), Observing our Changing Earth. Springer, Berlin, 387-396. doi:10.1007/978-3-540-85426-5-46.

Awange, J., Sharifi, M., Ogonda, G., Wickert, J., Grafarend, E., & Omulo, M. (2008b). The falling Lake Victoria water level: GRACE, TRIMM and CHAMP satellite analysis of the lake basin. Water Resource Management, 22 (7), 775-796. doi:10.1007/s112690079191y.

Becker, M., Llovel, W., Cazenave, A., Günter, A., & Crétaux, J.-F. (2010). Recent hydrological behavior of the East African great lakes region inferred from GRACE, satellite altimetry and rainfall observations.

Comptes Rendus Geoscience, 342 (3), 223–233. doi:10.1016/j.crte.2009 .12.010

Bettadpur, S. (2007). UTCSR Level-2 Processing Standards Document for Level- 2 Product Release 0004. Gravity Recovery and Climate Experiment (GRACE) Rev 3.1, GRACE 327–742 (CSR-GR-03-03), Center for Space Research, The University of Texas at Austin.

Brown, N. J., & Tregoning, P. (2010). Quantifying GRACE data contamination effects on hydrological analysis in the Murray-Darling Basin, southeast Australia. Australian Journal of Earth Sciences, 57, (3), 329-335, doi:http://dx.doi.org/10.1080/08120091003619241.

Cai, W., & Cowan, T. (2008). Dynamics of late autumn rainfall reduction over southeastern Australia. Geophysical Research Letters, 35, L09708. doi:10.1029/2008GL033727.

Cai, W., Cowan, T., & Sullivan, A. (2009). Recent unprecedented skewness towards positive Indian Ocean Dipole occurrences and their impact on Australian rainfall. Geophysical Research Letters, 36, L11705. doi:10.1029/2009GL037604.

Cai, W., van Rensch, P., Cowan, T., & Hendon, H. H. (2011). Teleconnection Pathways of ENSO and the IOD and the Mechanisms for Impacts on Australian Rainfall. Journal of Climate, 24, 39103923. doi: 10.1175/ 2011JCLI4129.1.

Cardoso, J. F., (1998). Blind signal separation: statistical principles. Proceedings of the IEEE, 10, 2009–2025, ISSN: 0018-9219, doi:10.1109/5.720250

86.

Cardoso, J. F., (1999). High-order contrasts for independent component analysis, Neural Computation, 11 (1), 157–192. doi:http://dx.doi.org/10.1162/089976699300016863.

Cardoso J. F., & Souloumiac, A. (1993). Blind beamforming for non-Gaussian signals. IEEE Proceedings, 362–370. doi:10.1.1.8.5684.

Chambers, D. P. (2006). Observing seasonal steric sea level variations with GRACE and satellite altimetry. Journal of Geophysics. Res. 111, C03010. doi:10.1029/2005JC002914.

Chen, J., Rodell, M., Wilson, C., & Famiglietti, J. (2005). Low degree spherical harmonic influences on Gravity Recovery and Climate Experiment (GRACE) water storage estimates. Geophysical Research Letters 32 (L14405). doi:10.1029/2005GL022964.

Chen, J.L., Wilson, C., & Seo, K-W. (2008). S2 tide aliasing in GRACE time-variable gravity solutions. Journal of Geodesy, 83 (7), 679–687. doi:10.1007/s00190-008-0282-1.

Comon, P. (1994). Independent component analysis, a new concept? Signal Process. 36 (3), 287–314. doi:http://dx.doi.org/10.1016/ 0165-1684(94)900299.

Döll, P., Kaspar, F., & Lehner, B. (2003). A global hydrological model for deriving water availability indicators: model tuning and validation. Journal of Hydrology 270 (1-2), 105-134. doi:10.1016/S00221694(02)002834.

Ellett, K. M., Walker, J. P., Western, A. W., & Rodell, M. (2006). A framework for assessing the potential of remote sensed gravity to provide new insight on the hydrology of the Murray-Darling Basin. Australian Journal of Water Resources, 10 (2), 89–101. ISSN: 1324-1583.

Fenoglio-Marc, L., Becker, M., Kusche, J., & Rietbroek, R. (2007). Leakage of Continental Hydrology in seawater mass change estimations from Space in the Mediterranean and Black Sea. In Proceedings of the Second Space for Hydrology Symposium, ESA Publications Division.

Flechtner, F. (2007). GFZ Level-2 processing standards document for level-2 product release 0004. GRACE 327–743, Rev. 1.0.

Flechtner, F., Bettadpur, S., Watkins, M., Kruizinga, G., & Tapely, B. (2010). GRACE science data system monthly report May 2010. http: // www.gfz-potsdam.de/pb1/op/grace/index_GRACE.html. Accessed October 2011.

Fleming, K., Awange, J., Kuhn, M., & Featherstone, W. E. (2011). Evaluating the TRMM 3B43 monthly precipitation product using gridded rain-gauge data over Australia. Australian Meteorological and Oceanographic Journal, 61, 171–184.

Forootan, E., & Kusche, J. (2011). Separation of global time-variable gravity signals into maximally independent components. Journal of Geodesy. doi:10.1007/s00190-011-0532-5.

Frappart, F., Ramillien, G., Leblanc, M., Tweed, S. O., Bonnet, M. P., & Maisongrande P. (2010a). An independent component analysis filtering approach for estimating continental hydrology in the GRACE gravity data. Remote Sensing of Environment, 115, 187-204. doi:10.1016/j.rse.2010.08.017.

Frappart F., Ramillien G., Maisongrande P., & Bonnet M.-P. (2010b). Denoising Satellite Gravity Signals by Independent Component Analysis. IEEE Geoscience and Remote Sensing Letters 7(3). doi:10.1109/LGRS.2009.2037837.

García-García, D., Ummenhofer, C. C., & Zlotnicki, V. (2011). Australian water mass variations from GRACE data linked to Indo-Pacific climate variability. Remote Sensing of Environment, 115 (9), 217-5-2183. doi:10.1016/j.rse.2011.04.007.

Güntner, A., Stuck, J., Döll, P., Schulze, K., & Merz, B. (2007). A global analysis of temporal and spatial variations in continental water storage. Water Resources Research 43, (W05416). doi:10.1029/2006WR005247.

Hannachi, A., Unkel, S., Trendafilov, N. T., & Jolliffe, I. T. (2009). Independent Component Analysis of Climate Data: A New Look at EOF Rotation. Journal of Climate 22, 2797–2812. doi:10.1175/2008JCLI2571.1.

Huffman, G., Adler, R., Bolvin, D., Gu, G., Nelkin, E., Bowman, K., Hong, Y., Stocker, E., & Wolff, D. (2007). The TRMM Multisatellite Precipitation Analysis (TMPA): Quasi-global, multiyear, combined-sensor precipitation estimates at fine scales. Journal of Hydrometeorology, 8 (1), 38-55. doi:10.1175/JHM560.1.

Hyvärinen, A. (1999a). Survey on independent component analysis. Neural Computing Surveys 2, 94–128.

Hyvärinen, A. (1999b). Fast and Robust Fixed-Point Algorithms for Independent Component Analysis. IEEE Transactions on Neural Networks 10, 626–634. doi:10.1109 /72.761722.

Hyvärinen, A., & Oja, E. (2000). Independent component analysis: algorithms and applications, Neural Networks, 13 (4-5), 411–430. doi:10.1016 /S0893-6080(00)00026-5.

Ilin, A., Valpola, H., & Oja, E. (2005). Semiblind source separation of climate data detects El Niño as the component with the highest interannual variability. In: Proceedings of the International Joint Conference on Neural Networks (IJCNN 2005), Montréal, Québec, Canada (2005) 1722-1727.

Jolliffe, I. T. (1989). Rotation of ill-defined principal components. Journal of the Royal Statistical Society. Series C (Applied Statistics) 38, 139–147. doi:10.2307/2347688.

Knudsen, P. (2003). Ocean tides in GRACE monthly averaged gravity fields. Space Sci Rev, 108, 261-270. doi:10.1023/A:1026215124036.

Kummerow, C., Barnes, W., Kozu, T., Shiue, J., & Simpson, J. (1998). The Tropical Rainfall Measuring Mission (TRMM) sensor package. Journal of Atmospheric and Oceanic Technology, 15 (3), 809-817. doi:10.1175/ 15200426(1998)015<0809:TTRMMT>2.0.CO;2.

Kummerow, C., Simpson, J., Thiele, O., Barnes,W., Chang, A., Stocker, E., Adler, R., Hou, A., Kakar, R., Wntz, F., Aschroft, P., Kozu, T., Hing, Y., Okamoto, K., Iguchi, T., Kuroiwa, H., Im, E., Haddad, Z., Huffman, G., Ferrier, B., Olson, W., Zipser, E., Smith, E., Wilheit, T., North, G., Krishnamurti, T., & Nakamura, K. (2000). The status of the Tropical Rainfall Measuring Mission (TRMM) after two years in orbit. Journal of Applied Meteorology, 39 (12), 1965-1982. doi:10.1175/15200450(2001)040<1965:TSOTTR>2.0.CO;2.

Kurtenbach, E. (2011). Entwicklung eines Kalman-Filters zur Bestimmung kurzzeitiger Variationen des Erdschwerefeldes aus Daten der Satellitenmission GRACE. PhD dissertation, Bonn University, Germany. *http://www.igg.uni-bonn.de/apmg/uploads/tx_ikgpublication/dissertation_kurtenbach.pdf*, accessed date: February 2012.

Kusche, J. (2007). Approximate decorrelation and non-isotropic smoothing of time-variable GRACE-type gravity field models. Journal of Geodesy, 81 (11), 733–749. doi:10.1007/s00190-007-0143-3.

Kusche, J., Schmidt, R., Petrovic, S., & Rietbroek, R. (2009). Decorrelated GRACE time-variable gravity solutions by GFZ, and their validation using a hydrological model. Journal of Geodesy, 83, 903-913. doi:10.1007/s00190-009-0308-3.

Leblanc, M., Tregoning, P., Ramillien, G., Tweed, S., & Fakes, A. (2009). Basin-scale, integrated observations of the early 21st century multiyear drought in southeast Australia. Water Resources Research, 45 (W04408). doi:10.1029/2008WR007333.

Lemoine, F., Luthcke, S., Rowlands, D., Chinn, D., Klosko, S., & Cox, C. (2007). The use of mascons to resolve time-variable gravity from GRACE. In: Tregoning, P., Rizos, C. (Eds.), Dynamic Planet. Springer, Berlin, 231-236. doi:10.1007/978-3-540-49350-1_35.

McGrath, G. S., Sadler, R., Fleming, K. M., Tregoning, P., Hinz, C. & Veneklaas, E. J. (2012). Tropical cyclones and the ecohydrology of Australia's recent continental-scale drought, Geophys. Res. Lett., doi:10.1029/2011GL050263, in press.

Mayer-Gürr, T., Eicker, A., & Kurtenbach, E. (2010). ITG-GRACE 2010 unconstrained monthly solutions, http://www.igg.uni-bonn.de/apmg /index.php?id=itg-grace2010, accessed date: October 2011.

Melachroinos, S. A., Lemoine, J.-M., Tregoning, P., & Biancale. R. (2009). Quantifying FES2004 S2 tidal model from multiple space-geodesy techniques, GPS and GRACE, over North West Australia. Journal of Geodesy, 83, 915923. doi:10.1007/s00190-009-0309-2.

Nicholls, N. (1991). Historical ENSO variability in the Australasian region. In El Niño Historical and Paleoclimatic aspects of the Southern Oscillation, H. F. Diaz and V. Markgraf (eds.), Cambridge Univ. Press, 151–173.

Nicholls, N. (2004). The changing nature of Australian droughts. Climatic Change, 63 (3), 323-336. doi:10.1023/B:CLIM.0000018515.46344.6d.

Nicholls, N. (2009). Local and remote causes of the southern Australian autumn-winter rainfall decline, 19582007. Climate Dynamics. doi:10.1007/

s00382-009-0527-6.

Papoulis, A. (1991). Probability, Random Variables, and Stochastic Processes. McGraw-Hill. ISBN-10: 0070484775.

Preisendorfer, R. (1988). Principal Component Analysis in Meteorology and Oceanography, Elsevier: Amsterdam. ISBN 10: 0444430148.

Ramillien, G., Cazenave, A., & Brunau, O. (2004). Global time variations of hydrological signals from GRACE satellite gravimetry. Geophysical Journal International, 158 (3), 813-826. doi:10.1111/j.1365246X.2004.02328.x.

Ray, R.D., & Luthcke, S.B. (2006). Tide model errors and GRACE gravimetry: towards a more realistic assessment. Geophys J. Int, 167(3):1055-1059. doi:10.1111/j.1365-246X.2006.03229.x.

Ray. R.D., & Ponte, R.M. (2003). Barometric tides from ECMWF operational analyses. Annales Geophysicae, 21, 1897-1910. doi:10.5194/angeo-21-1897-2003.

Rieser, D., Kuhn, M., Pail, R., Anjasmara, I. M., & Awange, J. (2010). Relation between GRACE-derived surface mass variations and precipitation over Australia. Australian Journal of Earth Sciences, 57 (7), 887–900. doi:10.1080/ 08120099.2010.512645.

Rietbroek, R., Brunnabend, S. E., Dahle, C., Kusche, J., Flechtner, F., Schrter, J., & Timmermann, R. (2009). Changes in total ocean mass derived from GRACE, GPS, and ocean modeling with weekly resolution. Journal of Geophysical Research, 114, C11004. doi:10.1029/ 2009JC005449.

Risbey, J. S., Pook, M. J., McIntosh, P. C., Wheeler, M. C., & Hendon, H. H. (2009). On the remote drivers of rainfall variability in Australia. Monthly Weather Review, 137, 3233-3253. doi:10.1175/2009MWR2861.1.

Rodell, M., & Famiglietti, J. (1999). Detectability of variations in continental water storage from satellite observations of the time dependent gravity field. Water Resources Research 35 (9), 2705-2723. doi:10.1029/1999WR900141.

Rodell, M., Houser, P., Jambor, U., Gottschalck, J., Mitchell, K., Meng, C.-J., Arsenault, K., Cosgrove, B., Radakovich, J., Bosilovich, M., Entin, J., Walker, J., Lohmann, D., & Toll, D. (2004). The Global Land Data Assimilation System. Bulletin of the American Meteorological Society, 85 (3), 381-394. doi:10.1175/ BAMS853381.

Ropelewski, C. F., & Jones, P. D. (1987). An Extension of the Tahiti-Darwin Southern Oscillation Index. Monthly Weather Review, 115 (9), 2161–2165. doi:10.1175/1520-0493(1987)115 < 2161:AEOTTS>2.0.CO;2.

Saji, N. H., Goswami, B. N., Vinayachandran, P. N., & Yamagata, T. (1999). A dipole mode in the tropical Indian Ocean. Nature, 401, 360363. doi:10.1038/43854.

Schmidt, R., Flechtner, F., Meyer, U., Neumayer, K. H., Dahle, C., Koenig, R., & Kusche, J. (2008). Hydrological signals observed by the GRACE satellites. Surveys in Geophysics 29, 319-334. doi:10.1007/s10712-008-9033-3.

Tapley, B., Bettadpur, S., Ries, J., Thompson, P., & Watkins, M. (2004a). GRACE measurements of mass variability in the Earth system. Science 305, 503-505. doi:10.1126/science.1099192.

Tapley, B., Bettadpur, S., Watkins, M., & Reigber, C. (2004b). The gravity recovery and climate experiment: Mission overview and early results. Geophysical Research Letters 31 (L09607). doi:10.1029/2004GL019920.

Thomas, M. (2002). Ocean induced variations of Earth's rotation-Results from a simultaneous model of global ocean circulation and tides, Ph.D. dissertation, 129 pp., Univ. of Hamburg, Hamburg, Germany.

Timbal, B., Arblaster, J., Braganza, K., Fernandez, E., Hendon, H., Murphy, B., Raupach, M., Rakich,C., Smith, I., Whan K., & Wheeler, M. (2010). Understanding the anthropogenic nature of the observed rainfall decline across South Eastern Australia. CAWCR technical report 2. ISBN: 978192160590.

Tregoning, P., Lambeck, K., & Ramillien, G. (2008). GRACE estimates of sea surface height anomalies in the Gulf of Carpentaria, Australia. Earth Planet. Sci. Lett., 271(14), 241244. http://dx.doi.org/10.1016/j.bbr.2011.03.031.

Tregoning, P., Watson, C-, Ramillien, G., McQueen, H., & Zhang, J. (2009). Detecting hydrologic deformation using GRACE and GPS. Geophys Res Lett 36:L15401. doi:10.1029/ 2009GL038718.

Trenberth, K. E., & Hoar, T. J. (1996). The 1990-1995 El Niño-Southern Oscillation Event Longest on Record. Geophysical Research Letters, 23 (1), 57–60. doi:10.1029/95GL03602.

Ummenhofer, C., England, M., McIntosh, P., Meyers, G., Pook, M., Risbey, J., Gupta, A., & Taschetto, A. (2009). What causes southeast Australias worst droughts? Geophysical Research Letters 36 (L04706). doi:10.1029/2008GL036801.

Ummenhofer, C. C., Gupta, A., Briggs, P. R., England, M. H., McIntosh, P. C., & Meyers, G. A., et al. (2011). Indian and Pacific Ocean influences on Southeast Australian drought and soil moisture. Journal of Climate. doi:10.1175/2010JCLI3475.1.

von Storch, H., & Zwiers, F. (1999). Statistical Analysis in Climate Research. Cambridge University Press, Cambridge. ISBN-10: 0521012309.

van Dijk, A. I. J. M., Renzullo, L. J., & Rodell, M. (2011). Use of Gravity Recovery and Climate Experiment terrestrial water storage retrievals to evaluate model estimates by the Australian water resources assessment system. Water Resources Research, 47, W11524. doi:10.1029/2011WR010714.

van Dijk, A. I. J. M., & Renzullo, L. J. (2011). Water resource monitoring systems and the role of satellite observations. Hydrol. Earth Syst. Sci., 15, 39-55.

Vinogradova, N. T., Ponte, R. M., Tamisiea, M. E., Quinn, K. J., Hill, E. M., & Davis, J. L. (2011). Self-attraction and loading effects on ocean mass redistribution at monthly and longer time scales. Journal of Geophysical Research, 116, C08041. doi:10.1029/2011JC007037.

Wahr, J., Molenaar, M., & Bryan, F. (1998). Time variability of the Earth's gravity field: Hydrological and oceanic effects and their possible detection using GRACE. Journal of Geophysical Research, 103 (B12), 30205-30229. doi:10.1029/98JB02844.

Werth, S., Güntner, A., Petrovic, S., & Schmidt, R. (2009a). Integration of GRACE mass variations into a global hydrological model. Earth and Planetary Science Letters, 27 (1-2), 166-173. doi:10.1016/j.epsl.2008.10.021.

Werth, S., Güntner, A., Schmidt, R., & Kusche, J. (2009b). Evaluation of GRACE filter tools from a hydrological perspective. Geophysical Journal of International, 179, 14991515. doi:10.1111/j.1365-246X.2009.04355.x.

Westra, S., Brown, C., Lall, U., & Sharma, A. (2007). Modeling multivariable hydrological series: Principal component analysis or independent component analysis? Water Resource. Res. 43, W06429. doi:10.1029/2006 WR005617.

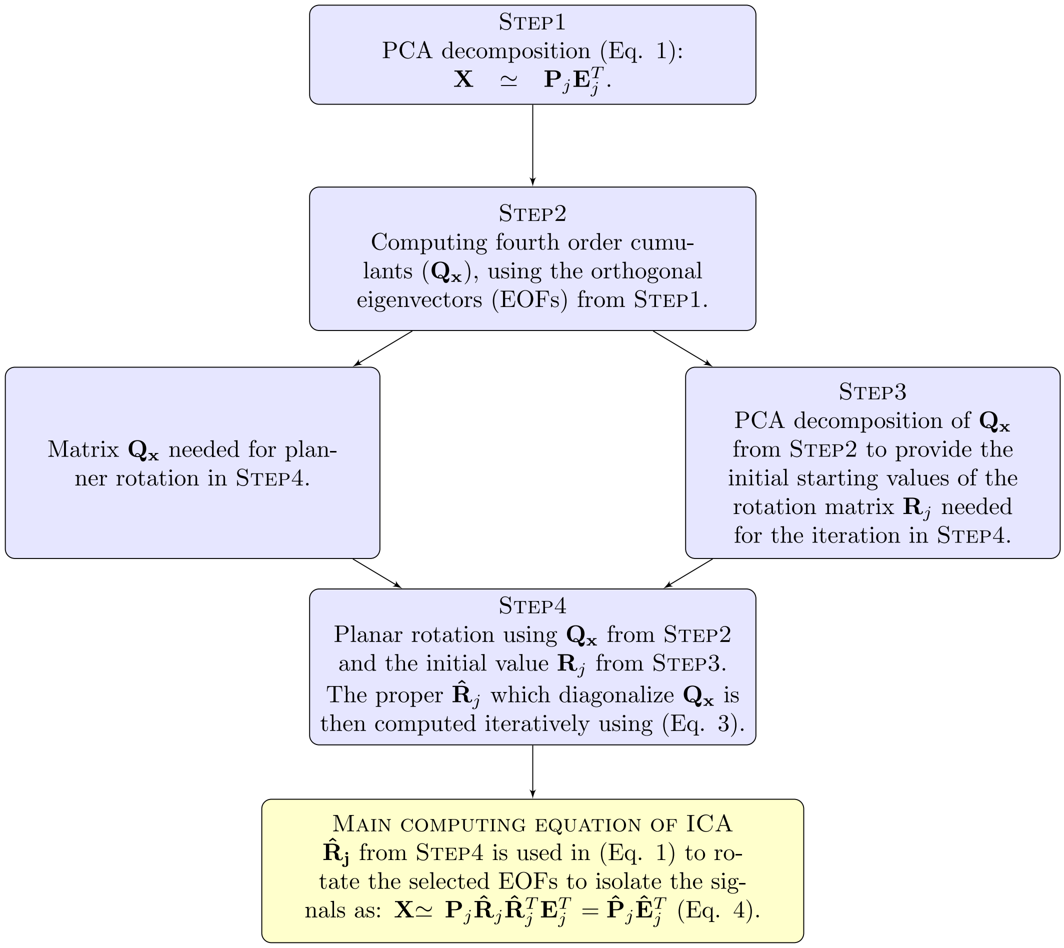

Figure 1: A schematic illustration of the ICA algorithm. For more details, we refer to Forootan and Kusche (2011).

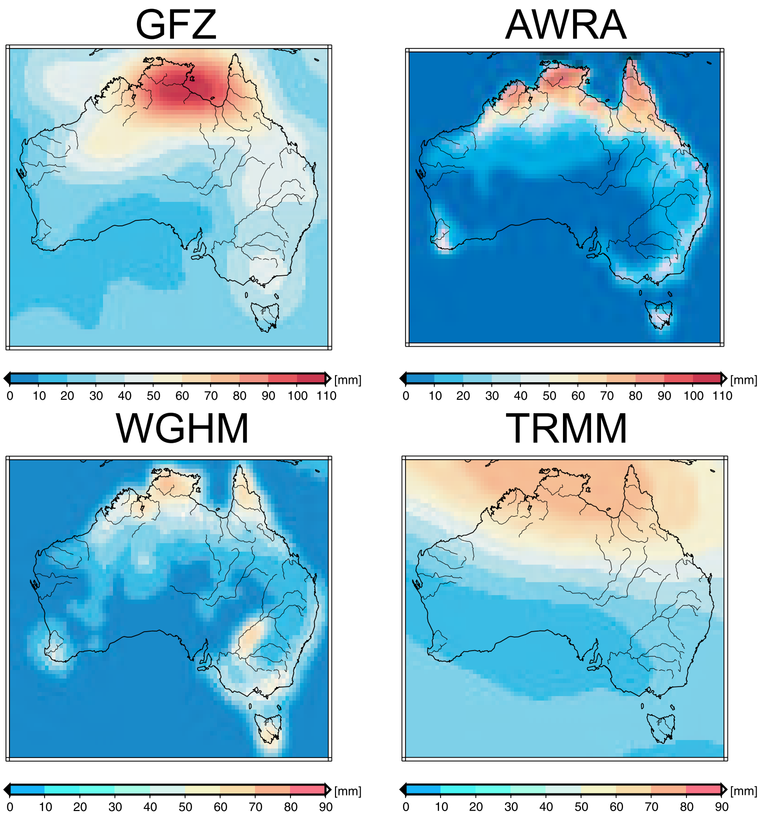

Figure 2: Comparing the signal variability (RMS) of the four main data sources used in this study after smoothing using the Kusche et al. (2009)'s DDK2 filter; GFZ-data (top-left), WGHM-data (bottom-left), AWRA-data (top-right) and TRMM-data (bottom-right).

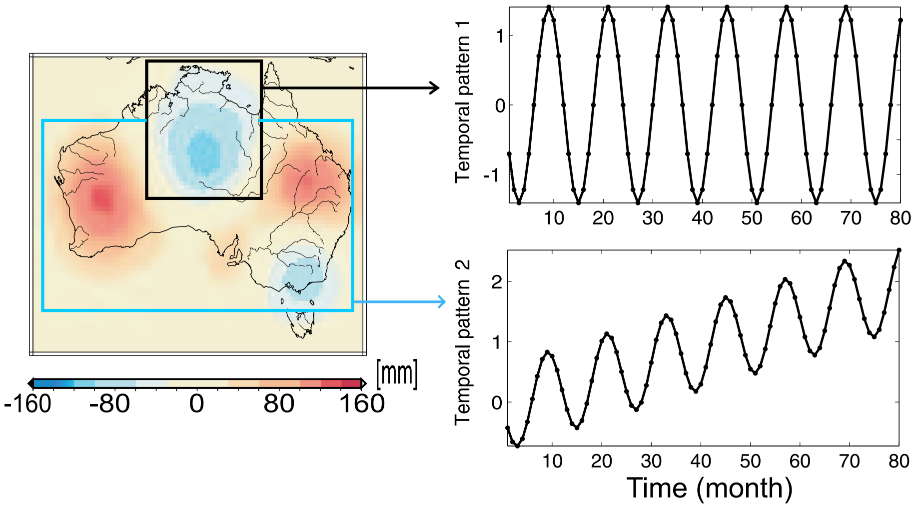

Figure 3: A synthetic example; the north of Australia exhibits only an annual signal while the west, east and southeast contain a superposition of a weaker annual signal and a linear trend. In order to reconstruct the synthetic data set, one should multiply the spatial pattern (left) with the temporal components (right).

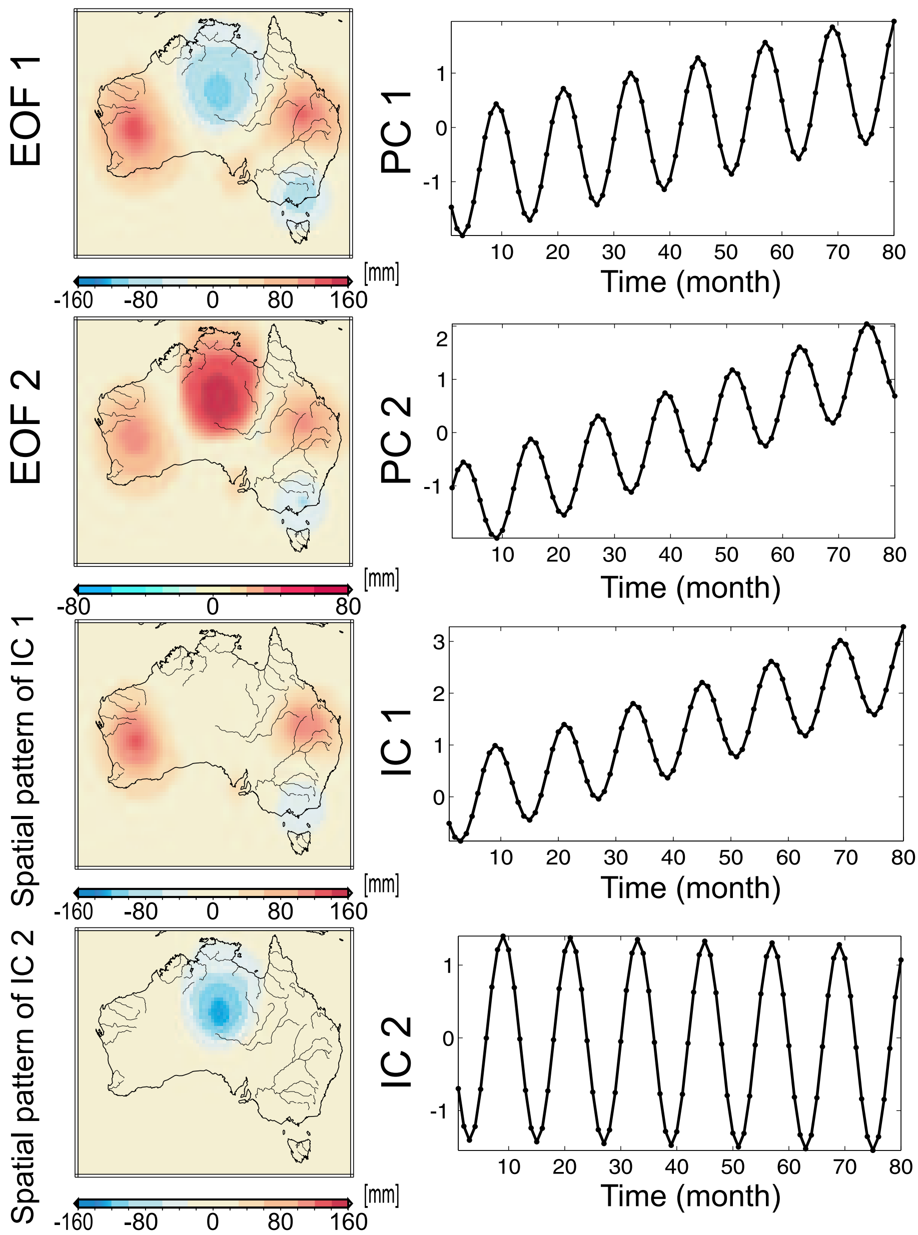

Figure 4: Separation of the simulated hydrological signals of Fig. (3) using PCA and ICA methods. The first two rows are related to the PCA results while the last 2 rows are related to the ICA results.

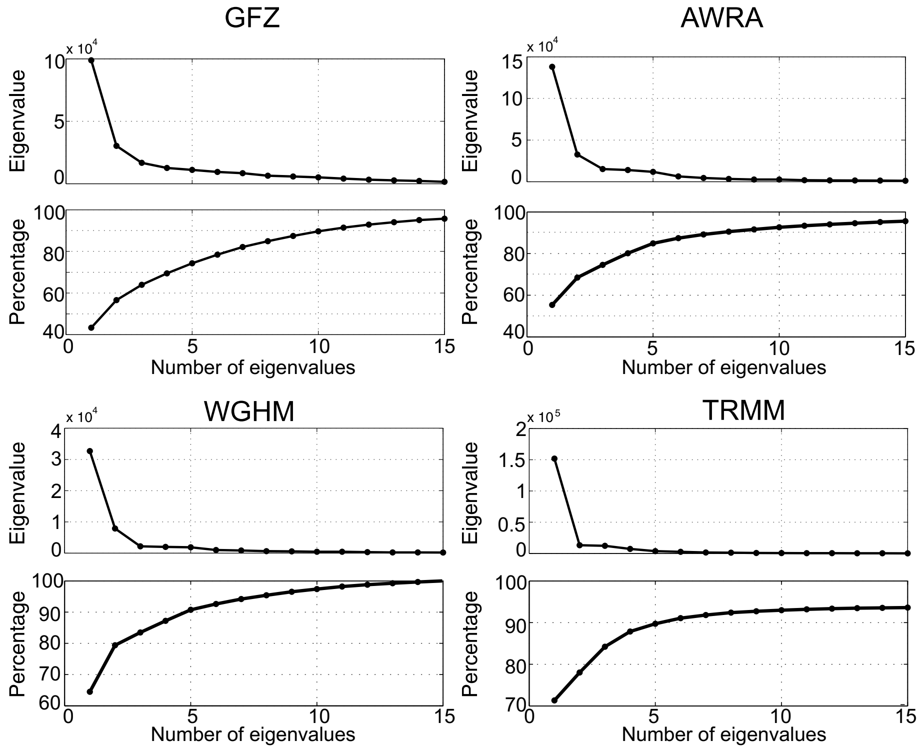

Figure 5: Eigenvalue results derived from implementing the PCA method on the GFZ, WGHM, AWRA and TRMM data sets are respectively shown in top-left, bottom-left, top-right and bottom right of the figure. Each sub-figure contains 2 graphs, including eigenvalue spectrum and cumulative variance contribution of the eigenvalues of each mentioned data sets.

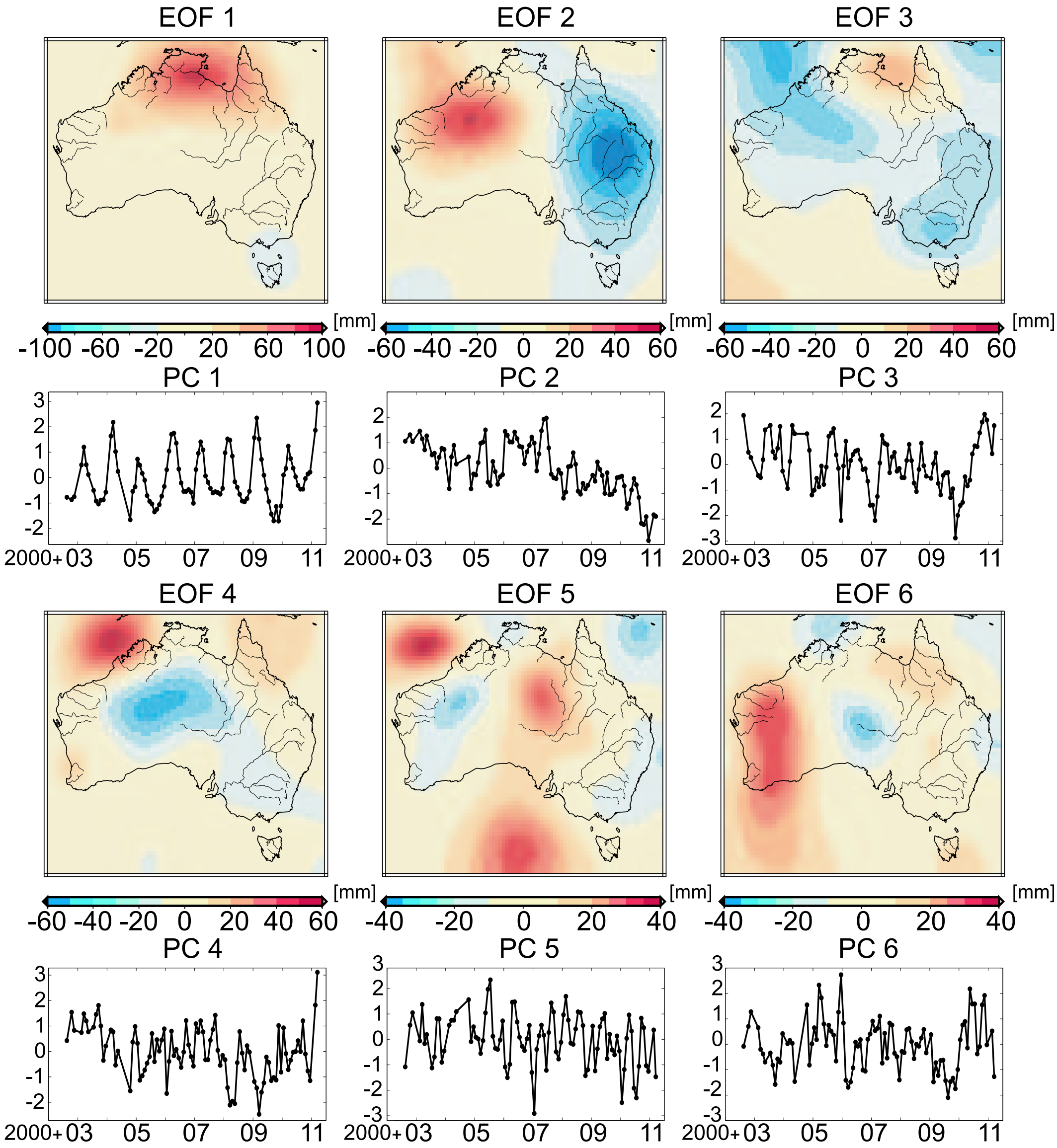

Figure 6: Results of PCA applied on total water storage maps of the GFZ center over Australia. The analysis covered the period from October 2002 to May 2011. The spatial anomalies are scaled using the standard deviation of their corresponding PCs to give millimeter unit. The temporal components are evolutions with standard deviation equal to 1.

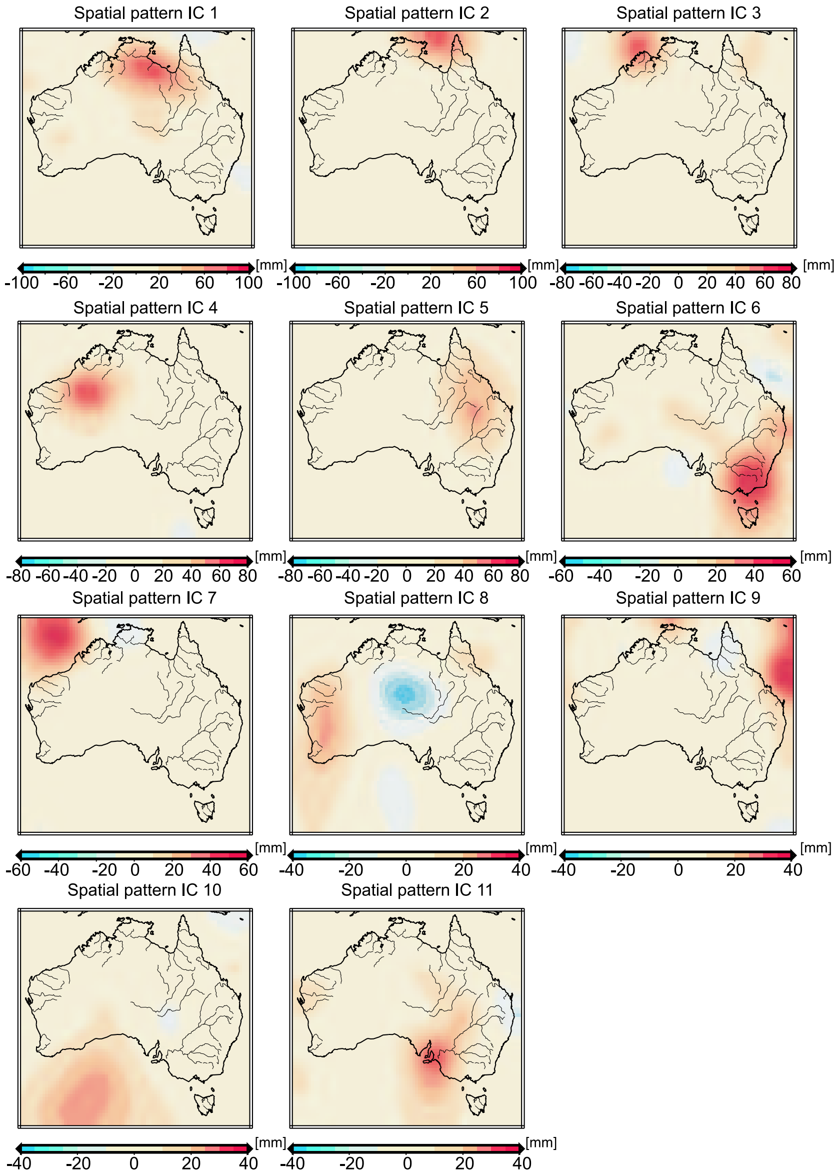

Figure 7: Results of the spatial ICA method applied to the GFZ total water storage maps over Australia. The spatial patterns are anomalies related to the GFZ data, which are scaled using the standard deviation of their corresponding temporal evolutions (shown in Fig. 8). The results are ordered according to the signal strength they represent such that they are comparable with those of PCA results in Fig. 6.

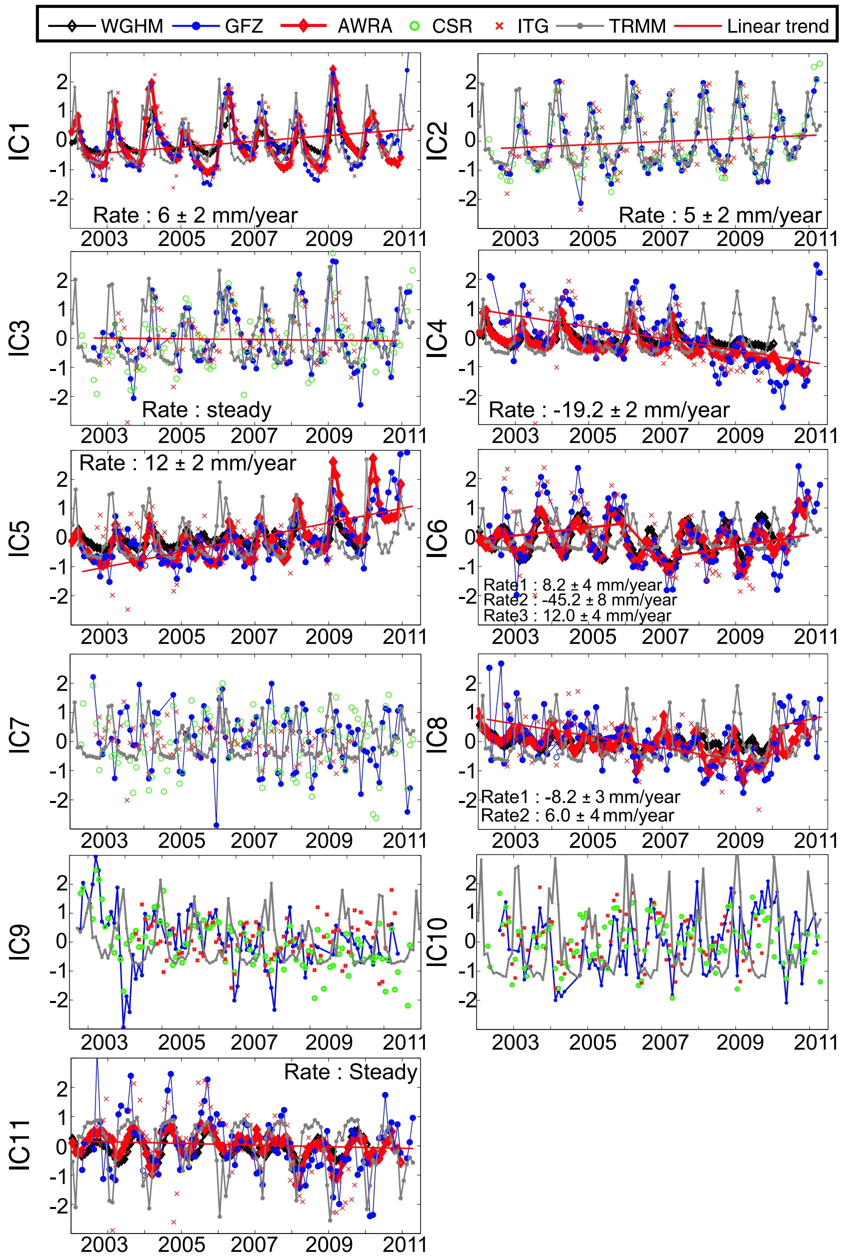

Figure 8: The evolutions of ICs corresponding to the spatial anomalies in Fig. 7 along with the projected temporal values of the CSR, ITG2010, WGHM, AWRA and TRMM data sets. For comparison purpose, the temporal evolutions are scaled using the standard deviation of the computed ICs of the GFZ data.

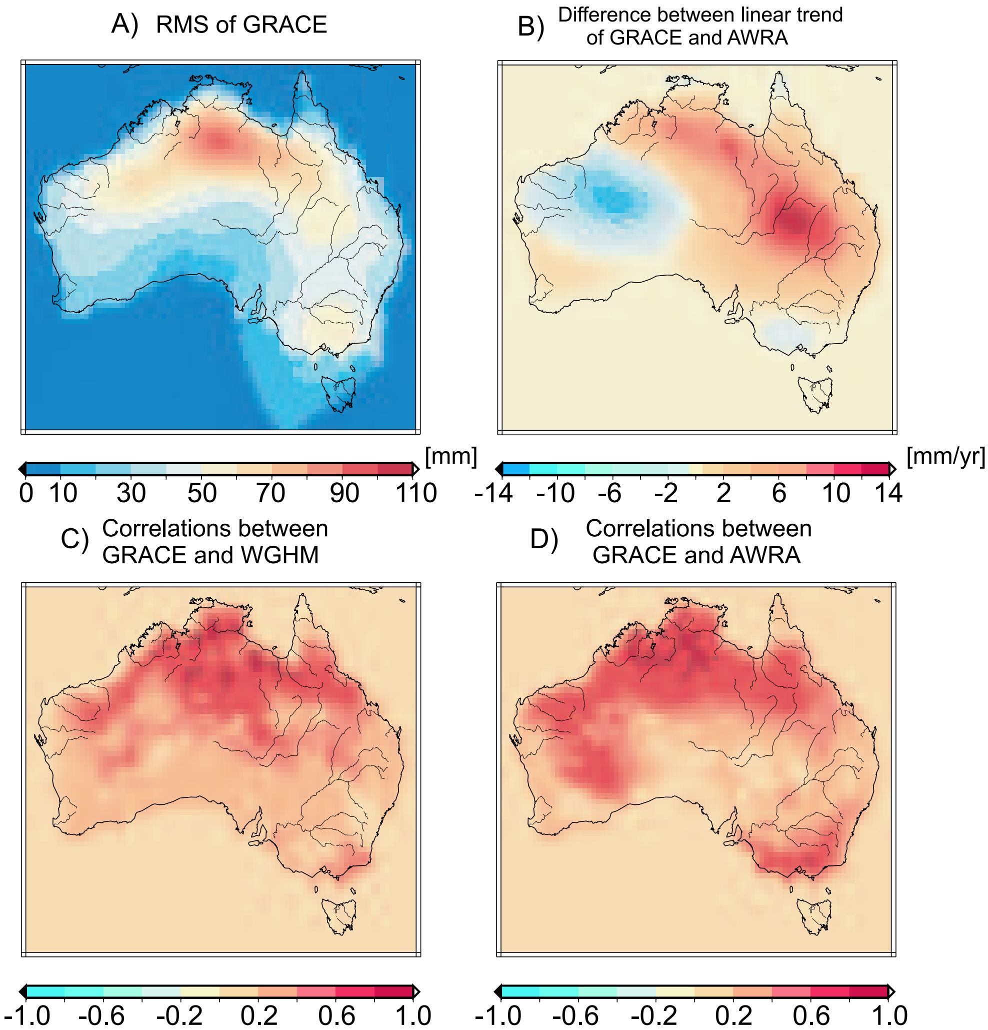

Figure 9: Overview of reconstructing GRACE-TWS variations over the Australian continent using ICA. (A) RMS of the reconstructed GRACE-TWS derived by multiplying the independent components of 1, 4, 5, 6, 8 and 10 of Fig. 7 to their corresponding temporal components in Fig. 8. (B) The difference between the linear trend computed from the ICA reconstructed time series of GRACE over the continent and the linear trend of AWRA, covering the period 2003 to 2011 (C) Temporal correlations between the ICA reconstructed time series of GRACE and the time series of WGHM for the period of 2003 to 2010. (D) Temporal correlations between the ICA reconstructed time series of GRACE and the time series of AWRA for the period of 2003 to 2011.

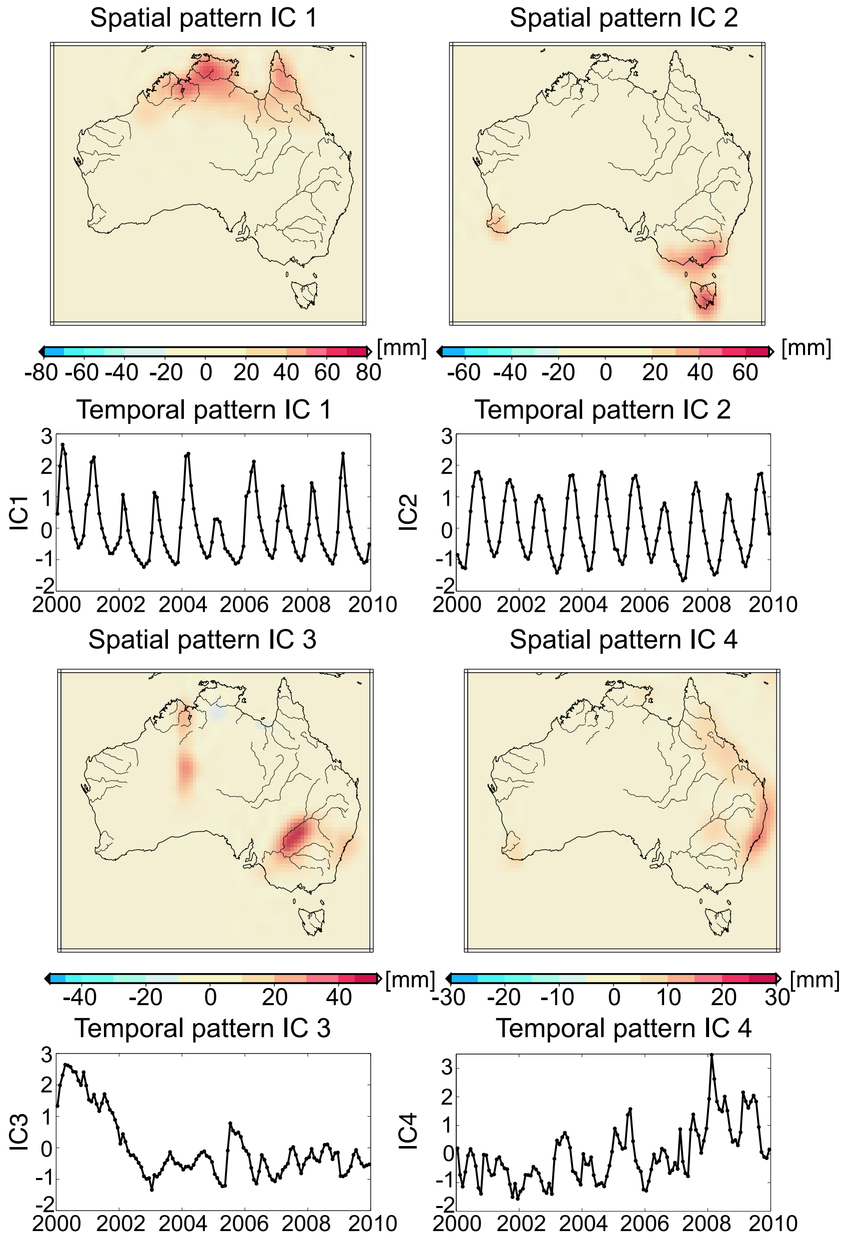

Figure 10: Overview of the performance of the ICA method on the WGHM hydrological data over Australia. The analysis covers the period between January 2000 and January 2010. The temporal components are scaled using their standard deviations such that they are unitless. The standard deviations are multiplied by spatial maps to give millimeter unit.

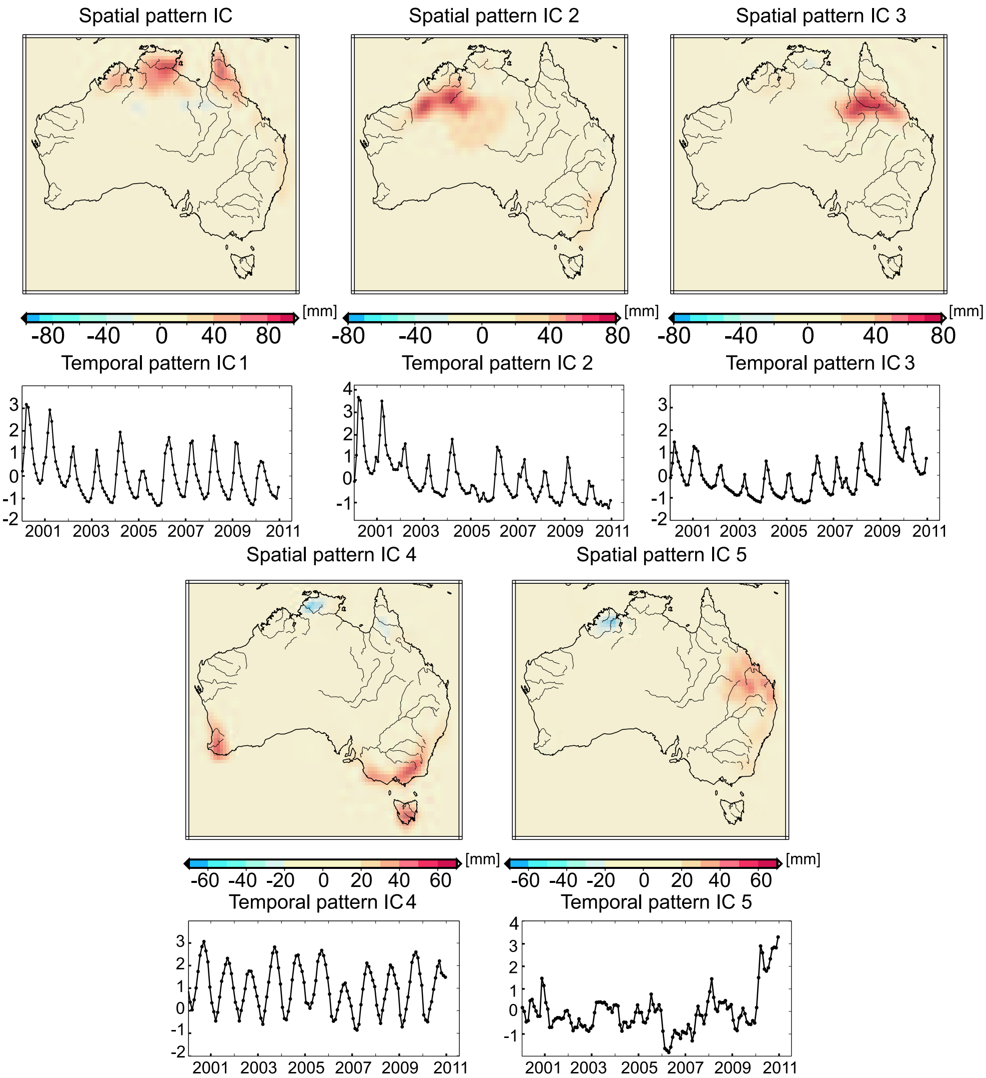

Figure 11: Overview of the performance of the ICA method on the AWRA hydrological data over Australia. The analysis covers the period between January 2000 and December 2010. The temporal components are scaled using their standard deviations such that they are unitless. The standard deviations are multiplied by spatial maps to give millimeter unit.

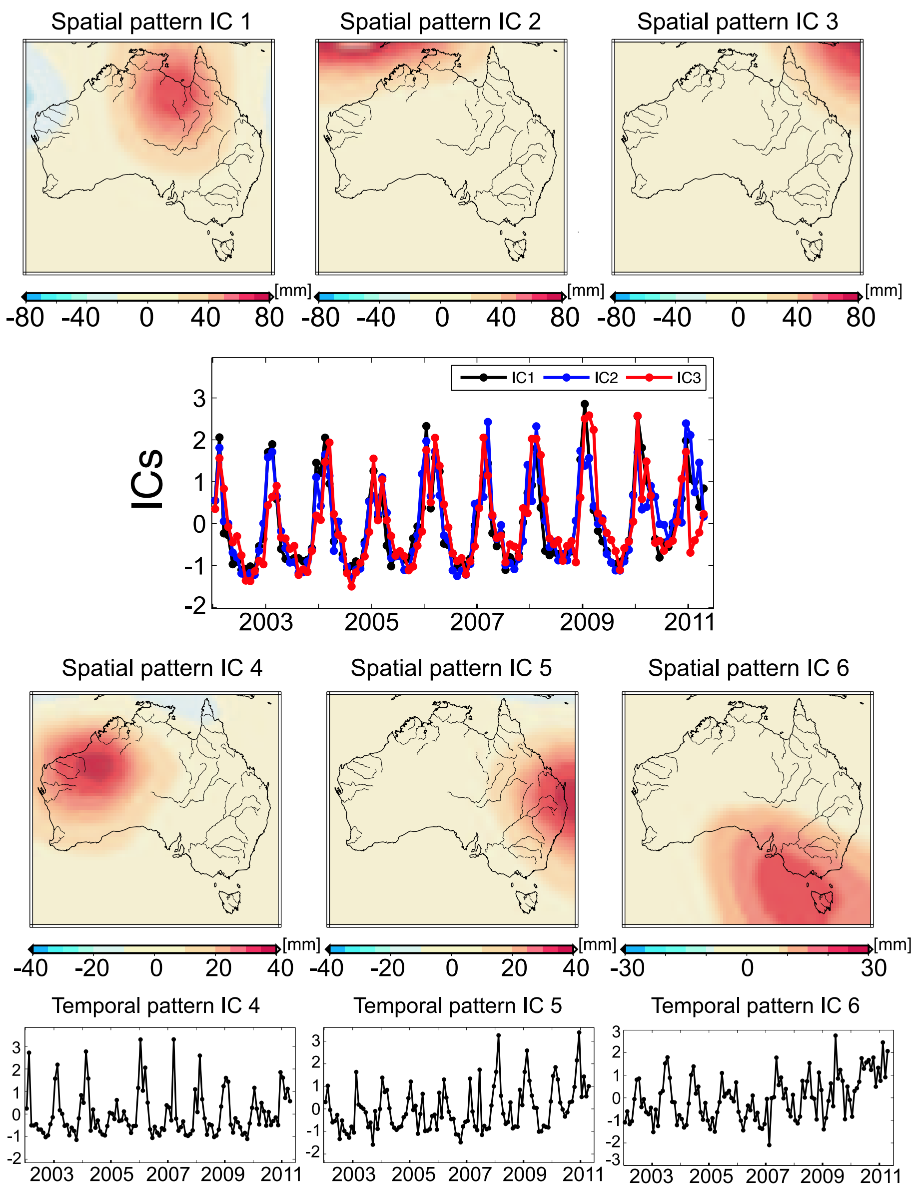

Figure 12: Overview of the performance of the ICA method on the TRMM data. The results are derived by rotating the first 5 EOFs, which contain more than 90% of the total variance of the data. The spatial patterns are anomalies that are scaled using the standard variation of their corresponding temporal evolutions. The temporal evolutions are unitless.

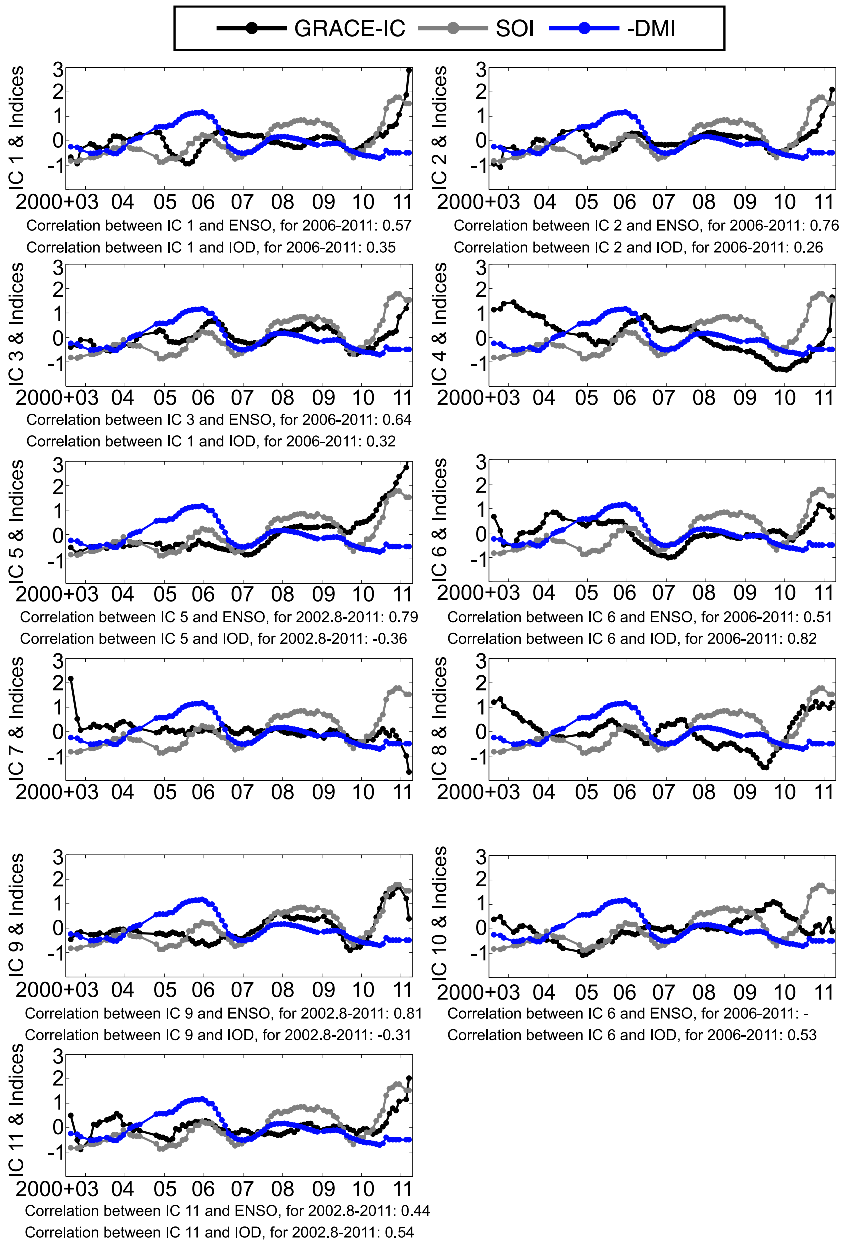

Figure 13: Overview of the temporal relation between ENSO and IOD with the Australian independent hydrological patterns derived from ICA of GFZ-TWS. In each graph, GFZ-ICs, SOI and -DMI indices are filtered using a 12-months moving average filter. The correlations are computed at 95% confidence level.